Cancer Science
The official journal of the Japanese Cancer Association JCA

Substrate-dependent bidirectional modulation of P-glycoprotein-mediated drug resistance by erlotinib

Kohji Noguchi,[1] Haruka Kawahara,[1] Airi Kaji,[1] Kazuhiro Katayama,[1] Junko Mitsuhashi[1,2] and Yoshikazu Sugimoto[1,2,3]

[1]Division of Chemotherapy, Graduate School of Pharmaceutical Sciences, Keio University, Minato-ku, Tokyo; [2]Division of Gene Therapy, Cancer Chemotherapy Center, Japanese Foundation for Cancer Research, Koto-ku, Tokyo, Japan

(Received January 7, 2009/Revised April 24, 2009/Accepted May 3, 2009/Online publication May 31, 2009)

Epidermal growth factor receptor tyrosine kinase inhibitors (EGFR-TKIs) inhibit the function of certain adenosine triphosphate (ATP)-binding cassette transporters, including P-glycoprotein/ABCB1 and breast cancer resistance protein (BCRP)/ABCG2. We previously reported an antagonistic activity of gefitinib towards BCRP. We have now analyzed the effects of erlotinib, another EGFR-TKI, on P-glycoprotein and BCRP. As with gefitinib, erlotinib effectively reversed BCRP-mediated resistance to SN-38 (7-ethyl-10-hydroxycamptothecin) and mitoxantrone. In contrast, we found that erlotinib effectively suppressed P-glycoprotein-mediated resistance to vincristine and paclitaxel, but did not suppress resistance to mitoxantrone and doxorubicin. Conversely, erlotinib appeared to enhance P-glycoprotein-mediated resistance to mitoxantrone in K562/MDR cells. This bidirectional activity of erlotinib was not observed with verapamil, a typical P-glycoprotein inhibitor. Flow cytometric analysis showed that erlotinib co-treatment restored intracellular accumulation of mitoxantrone in K562 cells expressing BCRP, but not in cells expressing P-glycoprotein. Consistently, erlotinib did not inhibit mitoxantrone efflux in K562/MDR cells although it did vincristine efflux in K562/MDR cells and mitoxantrone efflux in K562/BCRP cells. Intravesicular transport assay showed that erlotinib inhibited both P-glycoprotein-mediated vincristine transport and BCRP-mediated estrone 3-sulfate transport. Intriguingly, Lineweaver-Burk plot suggested that the inhibitory mode of erlotinib was a mixed type for P-glycoprotein-mediated vincristine transport whereas it was a competitive type for BCRP-mediated estrone 3-sulfate transport. Collectively, these observations indicate that the pharmacological activity of erlotinib on P-glycoprotein-mediated drug resistance is dependent upon the transporter substrate. These findings will be useful in understanding the pharmacological interactions of erlotinib used in combinational chemotherapy. (*Cancer Sci* 2009; 100: 1701–1707)

The ABC transporter protein P-glycoprotein/ABCB1 consists of two symmetrical halves connected by a linker region, with each half containing an ATP-binding domain and a six transmembrane domain.[1] P-glycoprotein has been investigated as a key cancer-related protein whose overexpression can lead to a tumor cell multidrug resistant phenotype.[1] P-glycoprotein transports out of cells various structurally unrelated chemotherapeutic agents, including vincristine (VCR), paclitaxel (PTX), doxorubicin (DOX), and mitoxantrone (MXR), thereby reducing their cytotoxic effects.[1] Overexpression of breast cancer resistance protein (BCRP)/ABCG2, a half-type ABC transporter with an ATP-binding domain and a six transmembrane domain, also modulates the efficacy of cancer chemotherapeutics,[2] rendering cancer cells resistant to various chemotherapeutic drugs. BCRP functions as a homodimer, transporting anticancer agents such as topotecan, irrinotecan, SN-38 (7-ethyl-10-hydroxycamptothecin), methotrexate, and MXR out of cells.[3]

A number of compounds have been tested for their ability to overcome ABC transporter-mediated drug resistance. Verapamil, cyclosporine A, and others have been identified as inhibitors of P-glycoprotein,[1,4,5] while fumitremorgin C (FTC), tamoxifen derivatives, and certain flavonoids inhibit BCRP.[3,6–8] These reagents directly interact with P-glycoprotein or BCRP and competitively interfere with transporter-substrate binding. This inhibition restores intracellular accumulation of the substrate drugs, effectively reversing drug resistance.

Epidermal growth factor receptor (EGFR) is a member of the ErbB/HER family of receptor tyrosine kinases and is frequently deregulated in human cancers, including non-small cell lung cancer (NSCLC), breast cancer, and glioblastomas.[9] As such, abnormal activation of EGFR signaling is a promising therapeutic target. Gefitinib and erlotinib, both EGFR inhibitory 4-anilinoquinazoline derivatives, are currently utilized in clinical chemotherapy, especially for lung cancer.[10] Extensive examination of functional interactions between BCRP and imatinib or gefitinib revealed that these kinase inhibitors are also substrates for BCRP with potent inhibitory activity against this ABC transporter.[11,12]

Erlotinib is an orally active EGFR tyrosine kinase inhibitor (TKI) with efficacy in NSCLC, ovarian cancer, pancreatic cancer, head and neck squamous cell cancer, and primary glioblastoma.[13] Erlotinib is approved in the United States for treatment of locally advanced or metastatic NSCLC after failure of at least one prior chemotherapy regimen.[14] It was also recently approved for use in combination with gemcitabine as a first line treatment for patients with locally advanced, unresectable, or metastatic pancreatic cancer.[15] Several clinical studies are planned to examine the combinational effects of erlotinib or gefitinib on conventional chemotherapy with various tumors. Detailed exploration of the pharmacological interaction between erlotinib and anticancer agents will contribute to optimize synergistic effects in such combination chemotherapy. Most recently, Shi *et al.* reported that erlotinib antagonized both P-glycoprotein- and BCRP-mediated drug resistances through direct inhibition of their efflux activities.[16,17] In the present study, we demonstrate that erlotinib inhibition of P-glycoprotein activity is substrate-specific.

Materials and Methods

Reagents. Erlotinib was kindly provided by F. Hoffmann-La Roche (Basel, Switzerland). SN-38 was provided by Yakult Honsha (Tokyo, Japan). FTC was purchased from Alexis (San Diego, CA, USA) and verapamil was purchased from Sigma-Aldrich (St. Louis, MO, USA). All other anticancer drugs were commercially available. MTT (3-[4,5-dimethyl-2-thiazolyl]-2,5-diphenyl-2H-tetrazolium bromide) was obtained from Wako Pure Chemical Industries, (Osaka, Japan).

Cells and drug sensitivity assay. PC-9 human NSCLC cells and K562 human myelogenous leukemia cells were cultured in DMEM and RPMI-1640 mediums, respectively, supplemented

[3]To whom correspondence should be addressed.
E-mail: sugimoto-ys@pha.keio.ac.jp

doi: 10.1111/j.1349-7006.2009.01213.x

with 7% fetal bovine serum and kanamycin (50 μg/mL) at 37 °C in a 5% CO_2 atmosphere. BCRP-expressing K562 cells (K562/BCRP), P-glycoprotein-expressing K562 cells (K562/MDR), and BCRP-expressing PC-9 cells (PC-9/BCRP) were established previously.[2] PC-9/MDR cells were established by the transduction of PC-9 with a HaMDR retrovirus harboring a Myc-tagged human *MDR1* cDNA in the Ha retrovirus vector as described previously.[18]

Erlotinib-induced growth inhibition of PC-9 and K562 cell lines was determined using a Coulter counter as described previously.[8] The effects of erlotinib on cell sensitivity to anticancer drugs were evaluated by MTT assay. Briefly, cells were seeded at 2×10^3 cells/well in 96-well plates. After incubation at 37 °C for 5 days in the presence of various concentrations of the drugs, MTT solution was added into each well and incubated for 4 h. An SDS/HCl solution was then added and incubated overnight to dissolve the formazan precipitate. Finally, OD570 was measured to estimate cell growth. IC_{50} values (the dosage of drug at which a 50% inhibition of cell growth was achieved) were determined from the growth inhibition curve. Reversal indices (RI50) were defined as the concentration of inhibitors (erlotinib, verapamil or FTC) that caused a 2-fold reduction in the IC_{50} values for anticancer drugs in each resistant cell as described previously.[8]

Intracellular accumulation of mitoxantrone. The effect of erlotinib on the cellular accumulation of MXR was determined by flow cytometry. K562, K562/BCRP, and K562/MDR cells (5×10^5 cells each) were incubated with 300 nmol/L MXR at 37 °C for 40 min in the absence or presence of erlotinib (0.1, 1, and 10 μmol/L), verapamil (1 and 10 μmol/L), or FTC (1 and 10 μmol/L). Cells were then washed with ice-cold PBS and subjected to fluorescence analysis using a BD LSR II system (Becton Dickinson, San Jose, CA, USA). MXR fluorescence was measured using a red 633-nm laser and a 660/20-band pass filter.

Intravesicular transport assay. Membrane vesicles of K562/MDR cells were prepared according to the method described previously.[19] The vesicular transport assay was done by a rapid centrifugation technique using ^{3}H-labeled VCR, MXR (American Radiolabeled Chemicals, St. Louis, MO, USA) and estrone 3-sufate (E1S) (Perkin-Elmer Life Sciences, Boston, MA, USA) as essentially described before.[12] In brief, the transport reaction mixture (50 μL volume; 50 mmol/L Tris-HCl [pH 7.4], 10 mmol/L $MgCl_2$, 250 mmol/L sucrose, 10 mmol/L phosphocreatine, 100 μg/mL creatine phosphokinase, with or without 3 mmol/L ATP, 100 nmol/L [^{3}H]VCR or 50 nmol/L [^{3}H]E1S, and membrane vesicles containing 10 μg protein) was kept on ice for 5 min and then reaction was started by incubation at 25 °C for 10 min. The reaction was terminated by an addition of 1 mL of ice-cold stop solution (10 mmol/L Tris-HCl [pH 7.4], 100 mmol/L NaCl, 250 mmol/L sucrose). The membrane vesicles were collected by centrifugation at 18 000 *g* for 10 min at 4 °C. The pellets were solubilized to measure their radioactivity levels by a liquid scintillation counter.

Cellular efflux assay. Cells (10^6/mL) were incubated with 0.2 μmol/L ^{3}H-labeled MXR or VCR for 30 min at 37 °C, washed twice with ice-cold PBS, and then suspended in ice-cold ^{3}H-free fresh normal growth medium. Aliquots of them were immediately mixed with ice-cold growth medium containing inhibitor (10 μmol/L each), stood in ice-water for 5 min, and then incubated at 37 °C for indicated times. Cell suspensions were centrifuged at 800 *g* for 5 min, and supernatants were collected to measure [^{3}H] radioactivity levels exported from cells by a liquid scintillation counter.

Results

Breast cancer resistance protein (BCRP)-mediated erlotinib resistance in PC-9 cells but not in K562 cells. The NSCLC cell line PC-9 harbors an *EGFR* gene with a 15-bp deletion[20] and shows enhanced sensitivity to the EGFR inhibitor gefitinib. K562 cells, on the other hand, express very little EGFR and do not show selective sensitivity to gefitinib inhibition.[12] We have observed that BCRP transports gefitinib and confers resistance to gefitinib only in gefitinib-sensitive cells such as PC-9, but not in non-sensitive cells such as K562.[2]

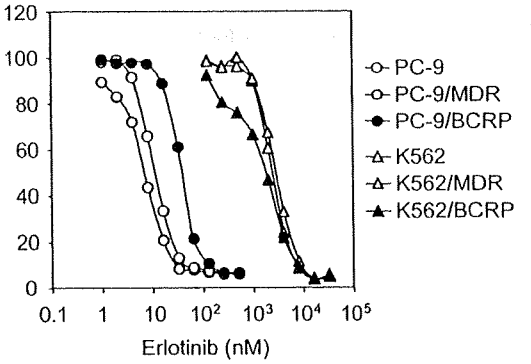

Fig. 1. Sensitivity of PC-9 and K562 cell lines to erlotinib. Cells were cultured for 5 days with increasing concentrations of erlotinib. Cell numbers were determined with a Coulter counter and cell growth inhibition curves (% of control) are shown. Data points are means ± SD calculated from triplicate determinations. Different symbols indicate specific cell lines: PC-9, open circles; PC-9/MDR, shaded circles; PC-9/breast cancer resistance protein (BCRP), filled circles; K562, open triangles; K562/MDR, shaded triangles; and K562/BCRP, filled triangles.

Sensitivity to erlotinib, another EGFR-TKI, was characterized in PC-9 and K562 cells expressing P-glycoprotein or BCRP (PC-9/MDR, PC-9/BCRP, K562/MDR, and K562/BCRP). Cells were incubated with erlotinib and the ratio of cell growth inhibition was used to determine IC_{50} values for each cell line. As shown in Figure 1, erlotinib inhibited PC-9 cell growth at nanomoler concentrations (IC_{50}, ~10 nmol/L), whereas K562 cells grew normally in the presence of such lower concentrations of erlotinib (IC_{50}, 2.4 μmol/L). Thus, PC-9 cells were more sensitive to erlotinib than K562 cells. Interestingly, PC-9/BCRP cells were approximately 2.8-fold more resistant to erlotinib than parental PC-9 and PC-9/MDR cells. The sensitivity of K562/MDR or K562/BCRP cells in erlotinib was almost identical to that of the parental K562 cells. Consistent with the published results for gefitinib,[12] the present findings indicate that BCRP expression confers resistance to erlotinib in PC-9 cells but not in K562 cells.

Effects of erlotinib on BCRP-mediated drug resistance. Gefitinib acts as an inhibitor for transporters and reverses P-glycoprotein- and BCRP-mediated resistance to various anticancer drugs.[12] K562 cells were not sensitive to the selective cytotoxicity of erlotinib-mediated EGFR inhibition. Therefore, we used K562/MDR and K562/BCRP cell lines to test such erlotinib reversal activity affecting P-glycoprotein- and BCRP-mediated drug resistance. K562/BCRP cells showed significant resistance to SN-38 (~25-fold) and MXR (~7-fold). Erlotinib co-treatment effectively reversed BCRP-mediated resistance to both drugs (Fig. 2a,b).

The dose dependency of this erlotinib-mediated suppressive effect was also analyzed. Erlotinib at 1.5 μmol/L (Fig. 2, open squares) effectively eliminated BCRP-mediated resistance to SN-38 and MXR. In similar experiments using erlotinib or FTC as a control inhibitor of BCRP-mediated resistance, both drugs reduced resistance to SN-38 and MXR in a dose-dependent manner (Fig. 2c,d). BCRP-mediated drug resistance reversal abilities for erlotinib and FTC were calculated as the RI50 value that caused a 2-fold reduction in the IC_{50} for each drug. As

doi: 10.1111/j.1349-7006.2009.01213.x

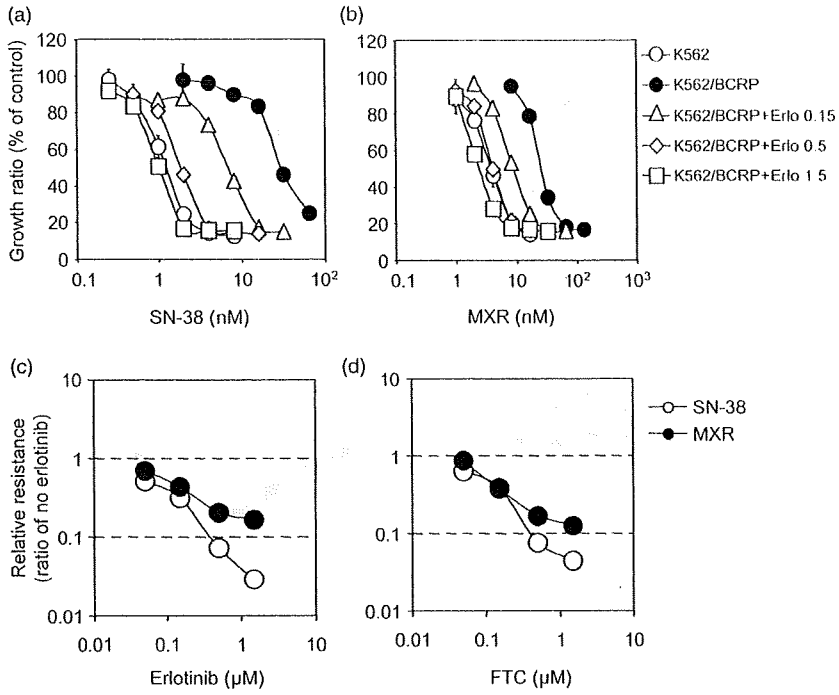

Fig. 2. Reversal of breast cancer resistance protein (BCRP)-mediated drug resistance in K562/BCRP cells. The sensitivity of K562/BCRP cells to SN-38 (7-ethyl-10-hydroxycamptothecin) (a) and mitoxantrone (MXR) (b) was determined in the presence of different concentrations of erlotinib: 0.15 μmol/L, open triangles; 0.5 μmol/L, open diamonds; 1.5 μmol/L, open squares. Cell growth inhibition following 5 days of culture was determined using the MTT assay. Growth inhibition curves were established from the means ± SD of triplicate determinations. Similar experiments were performed in the presence of fumitremorgin C (FTC) and the relative resistance to SN-38 (open circles) or MXR (filled circles) in the presence erlotinib (c) or FTC (d) was calculated as the ratio of an IC_{50} value in the presence of an inhibitor divided by the IC_{50} value without inhibitors.

Table 1. Values of RI50 (μM) to BCRP-mediated resistance

		Erlotinib	FTC
BCRP	MXR	0.10 ± 0.01	0.19 ± 0.02
	SN-38	0.05 ± 0.01	0.09 ± 0.02

Means ± SD. Experiments were performed in triplicate.
BCRP, breast cancer resistance protein; FTC, fumitremorgin C; MXR, mitoxantrone; RI50, reversal indices; SN-38, 7-ethyl-10-hydroxycamptothecin.

shown in Table 1, the RI50 values of erlotinib to SN-38 and MXR were 0.05 and 0.1 μmol/L, respectively. Interestingly, SN-38 resistance was more susceptible to erlotinib than MXR resistance. The RI50 values of erlotinib were comparable with those of FTC. Thus, erlotinib and FTC appeared to have equivalent inhibitory activities against BCRP-mediated drug resistance.

Distinct modulation of P-glycoprotein-mediated drug resistance by erlotinib. Although our experiments did not show obvious erlotinib-resistance in PC-9/MDR cells, we examined the effects of erlotinib on P-glycoprotein-mediated drug resistance in K562 cells based on reports that gefitinib was able to reverse P-glycoprotein-mediated drug resistance. MTT assays showed that K562/MDR cells were resistant to VCR (relative resistance was ~360-fold), PTX (~1000-fold), DOX (~25-fold), and MXR (~9-fold) (data not shown). We next examined the effects of erlotinib at various concentrations. Representative results showing K562/MDR cell resistance to VCR and to MXR are presented in Figure 3(a,b). As previously reported for gefitinib,[12] erlotinib effectively reversed VCR-resistance in K562/MDR cells (Fig. 3a). However, when K562/MDR cells were co-treated with erlotinib at 1.5 μmol/L, cells still showed significant resistance to VCR (~32-fold, open squares), whereas erlotinib completely eliminated BCRP-mediated resistance to SN-38 (as shown in Fig. 2a). Higher concentrations of erlotinib (over 5 μmol/L) were required for complete reversal of P-glycoprotein-mediated VCR-resistance. Moreover, we unexpectedly found that in K562/MDR cells, erlotinib did not reverse resistance to MXR. Conversely, erlotinib at concentrations of 0.15–1.5 μmol/L shifted the growth inhibition curve to the right (Fig. 3b), suggesting that erlotinib treatment stimulated P-glycoprotein-mediated resistance to MXR.

Variations in IC_{50} values for co-treatments with erlotinib or verapamil and each anticancer drug were determined in order to compare their ability to inhibit P-glycoprotein-mediated resistance phenotypes (Fig. 3c,d). This assessment showed that verapamil, a typical MDR-inhibitor, actually suppressed resistance to a series of drugs (VCR, PTX, DOX, and MXR) mediated by P-glycoprotein at similar concentrations (Fig. 3d). In contrast, erlotinib-induced reversal of P-glycoprotein-mediated resistance was different for individual anticancer drugs. Co-treatment of K562/MDR cells with erlotinib at 1.5 μmol/L, which significantly suppressed resistance to both VCR and PTX (Fig. 3c, open squares and open diamonds respectively), did not affect resistance to DOX (Fig. 3c, filled triangles). Thus, the P-glycoprotein-mediated resistance to DOX was less sensitive to erlotinib-mediated inhibition compared with resistance to VCR.

Remarkably, resistance to MXR was hardly affected by erlotinib, even at 5 μmol/L. Conversely, erlotinib co-treatment (0.15–1.5 μmol/L) increased MXR resistance in K562/MDR cells (Fig. 3c, filled circles). We confirmed these bidirectional effects of erlotinib on P-glycoprotein-mediated resistance with two different methods: the MTT assay and a cell growth assay that counted cell numbers using a Coulter counter (data not shown). Both methods suggested that at clinical concentrations, erlotinib potentiated P-glycoprotein-mediated resistance to MXR in K562/MDR cells.

As shown in Table 2, calculated RI50 values of erlotinib treatment for P-glycoprotein-mediated resistance to each anticancer drug clearly showed that P-glycoprotein-mediated resistance to DOX and MXR was approximately 10-fold less sensitive to erlotinib than observed for VCR and PTX. Conversely, verapamil reversed resistance to each of these drugs at comparable concentrations (RI50, 0.11–0.18 μmol/L). Therefore, the effects of erlotinib on P-glycoprotein-mediated resistance were quite different from those observed for verapamil and also from erlotinib

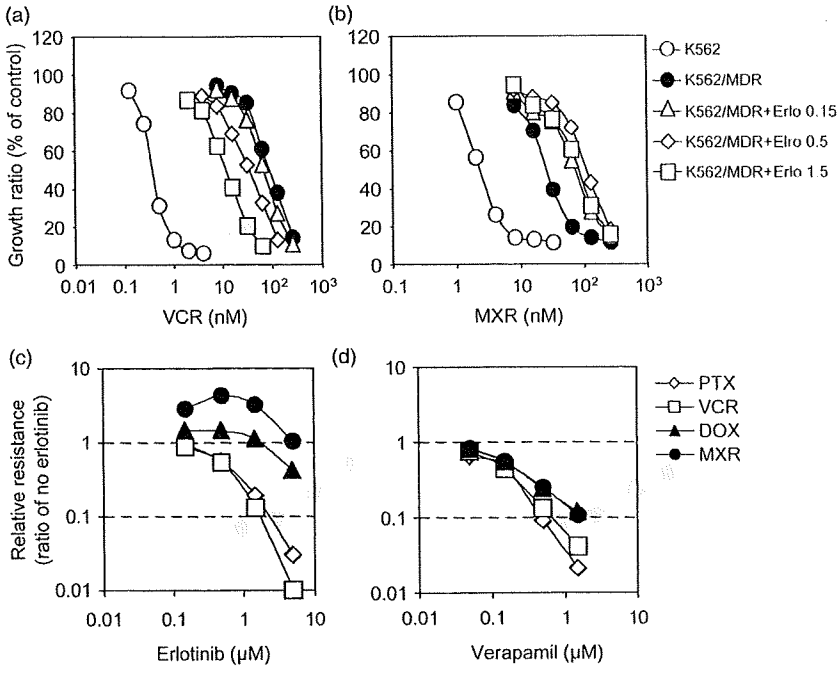

Fig. 3. Reversal of P-glycoprotein-mediated drug resistance in K562/MDR cells. The sensitivity of K562/MDR cells to vincristine (VCR) (a) and mitoxantrone (MXR) (b) was determined in the presence of different concentrations of erlotinib: 0.15 μmol/L, open triangles; 0.5 μmol/L, open diamonds; 1.5 μmol/L, open squares. The sensitivity of K562 (open circles) and K562/MDR (filled circles) cells to VCR (a) and MXR (b) was also determined in the absence of erlotinib. Cell growth inhibition following 5 days of culture was determined using the MTT assay. Growth inhibition curves were established from the means ± SD of triplicate determinations. Similar cell growth inhibition assays were performed using paclitaxel (PTX) and doxorubicin (DOX) in the presence of erlotinib or verapamil (0.05, 0.15, 0.5, and 1.5 μmol/L). Relative resistance to PTX (open diamonds), VCR (open squares), DOX (filled triangles), and MXR (filled circles) in the presence erlotinib (c) or verapamil (d) were calculated as the ratio of an IC_{50} value in the presence of an inhibitor divided by the IC_{50} value without inhibitors.

Table 2. Values of RI50 (μM) to P-glycoprotein-mediated resistance

		Erlotinib	Verapamil
MDR	MXR	–	0.18 ± 0.01
	DOX	4.0 ± 0.2	0.18 ± 0.01
	VCR	0.37 ± 0.02	0.11 ± 0.02
	PTX	0.44 ± 0.02	0.13 ± 0.03

Means ± SD. Experiments were performed in triplicate.
DOX, doxorubicin; MXR, mitoxantrone; PTX, paclitaxel; RI50, reversal indices; VCR, vincristine.

effects on BCRP-mediated resistance. Collectively, these data indicated that inhibitory ability of erlotinib was dependent upon the specific substrate in the P-glycoprotein-mediated resistance phenotype.

Effects of erlotinib on intracellular accumulation of mitoxantrone in cells expressing ABC transporters. The observations described above suggest that erlotinib may inhibit cellular efflux of MXR mediated by the ABC transporter BCRP, but not by P-glycoprotein. The effects of erlotinib on the intracellular accumulation of MXR in BCRP- or P-glycoprotein-expressing K562 cells were examined by flow cytometric analysis. After incubating cells with 300 nmol/L MXR for 40 min, fluorescence intensity indicative of MXR uptake significantly increased in K562 cells, but only moderately increased in K562/BCRP and K562/MDR cells (Fig. 4a,b). These results indicated that BCRP and P-glycoprotein exported MXR out of the cells.

Erlotinib co-treatment enhanced MXR cellular fluorescence intensity in K562/BCRP cells in a dose-dependent manner (Fig. 4c). The intracellular accumulation levels of MXR were determined by measuring peak fluorescence values at each point to compare efficacies of each inhibitor (Fig. 4e, with K562/BCRP cells shown as open columns). FTC or erlotinib at 10 μmol/L caused a similar enhancement of MXR accumulation in K562/BCRP cells, suggesting that erlotinib suppressed MXR efflux through BCRP with an efficacy that was similar to FTC.

Next, similar experiments were performed in K562/MDR cells to determine whether erlotinib modulates P-glycoprotein-mediated MXR transport (Fig. 4d). Consistent with its other effects on the P-glycoprotein-mediated resistance phenotype, co-treatment with erlotinib at concentrations up to 10 μmol/L did not enhance MXR fluorescence intensity in K562/MDR cells (Fig. 4d,e). Instead, erlotinib at 0.1–1 μmol/L slightly reduced MXR fluorescence intensity, suggesting that erlotinib treatment stimulated the MXR efflux mediated by P-glycoprotein. This effect of erlotinib on P-glycoprotein was in agreement with a stimulation of MXR resistance by erlotinib co-treatment in K562/MDR cells (Fig. 3b). Taken together, these results indicate that erlotinib suppressed MXR efflux mediated by BCRP, but not by P-glycoprotein, in K562 cells.

Effects of erlotinib on P-glycoprotein-mediated transport. Next we examined an effect of erlotinib on cellular efflux of VCR and MXR in K562/MDR and K562/BCRP cells (Fig. 5). Time course–dependent extracellular accumulations of [^{3}H]VCR in the supernatants of K562/MDR cell samples were clearly suppressed by both erlotinib and verapamil at 10 μmol/L (Fig. 5a, closed and open circles respectively). These data indicated that P-glycoprotein-mediated VCR efflux was inhibited by erlotinib. However, similar experiments using MXR as a transporter substrate showed that erlotinib did not inhibit MXR efflux in K562/MDR cells (Fig. 5b) despite the fact that erlotinib suppressed BCRP-mediated MXR efflux like FTC (Fig. 5c). These observations indicated that erlotinib sensitivity of P-glycoprotein was dependent on the transporter substrate type.

To understand the possible mechanism for substrate-dependent erlotinib inhibition on P-glycoprotein, intravesicular transport assay was performed to analyze kinetics of erlotinib inhibition on P-glycoprotein-mediated drug transport *in vitro* using membrane vesicles from K562/MDR cells. As shown in Figure 6a, ATP-dependent [^{3}H]VCR transport was actually inhibited by erlotinib in a dose-dependent manner, although with less efficiency than by verapamil (IC_{50} values of erlotinib and verapamil were 2 and 0.2 μmol/L respectively). Moreover, Lineweaver-Burk plot analysis showed that the inhibitory mode of erlotinib for P-glycoprotein-mediated VCR transport was a mixed type while

doi: 10.1111/j.1349-7006.2009.01213.x

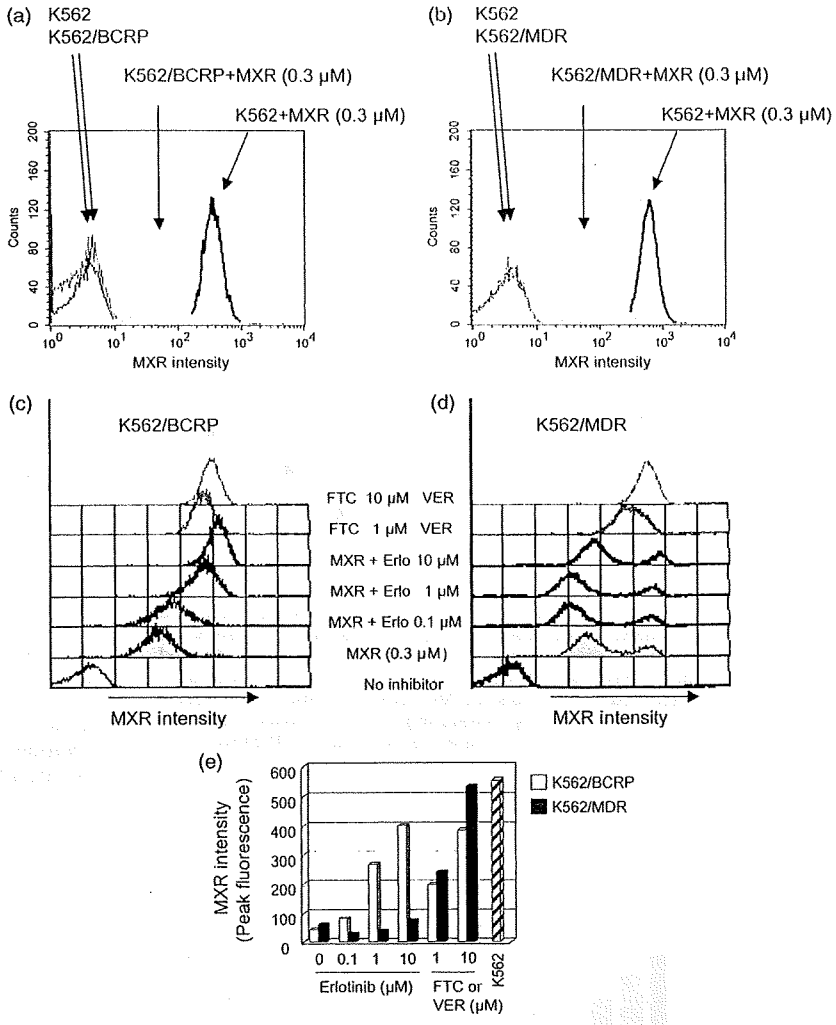

Fig. 4. Effects of erlotinib on the intracellular accumulation of MXR. Breast cancer resistance protein (BCRP)- and P-glycoprotein-mediated efflux reduces intracellular accumulation of mitoxantrone (MXR) (a and b). K562, K562/BCRP (a), and K562/MDR (b) cells were incubated for 40 min in the absence or presence of 0.3 μmol/L MXR, and then washed as described in 'Materials and Methods'. Cellular uptake of MXR was determined as fluorescence intensity of MXR measured by flow cytometry. Modulation of MXR accumulation by erlotinib (c and d). K562/BCRP (c) and K562/MDR (d) cells were incubated with MXR (0.3 μmol/L) and inhibitory agents, erlotinib (0, 0.1, 1, and 10 μmol/L) or the selective inhibitor fumitremorgin C (FTC) (c, shaded lines) or verapamil (VER) (d, shaded lines) at 1 and 10 μmol/L for 40 min. Cellular uptake of MXR was measured as described above, and MXR levels were determined as peak fluorescence values. Intracellular MXR accumulation patterns are shown as change of peak fluorescence values (e). A peak fluorescence for K562 cells is shown as control (slash column).

that of verapamil was a competitive type (Fig. 6b). The calculated *Vmax* values (pmol/mg/min) were 18 in control, 1.8 in erlotinib (2 μmol/L)-treated, and 17.8 in verapamil (0.2 μmol/L)-treated samples respectively, and the calculated *Ki* value of verapamil was 270 nmol/L.

The erlotinib effect on BCRP was also analyzed using membrane vesicles from K562/BCRP cells and [^{3}H]estrone 3-sulfate (E1S) as a transporter substrate of BCRP in an *in vitro* system. These experiments showed that both erlotinib and FTC inhibited BCRP-mediated E1S transport with similar efficiency (IC_{50} values of erlotinib and FTC were 0.13 and 0.25 μmol/L respectively) (Fig. 6c). In this case, Lineweaver-Burk plot analysis indicated that the calculated *Vmax* values (pmol/mg/min) in control, erlotinib (0.13 μmol/L)-treated, and FTC (0.25 μmol/L)-treated samples appeared to be at similar levels (20 in control, 18.9 in erlotinib treated, and 19.5 in FTC-treated, respectively). The calculated *Ki* value of erlotinib was about 150 nmol/L and that of FTC was about 550 nmol/L to BCRP-mediated E1S transport. Therefore, the inhibitory mode of erlotinib for BCRP-mediated E1S transport looked a competitive type (Fig. 6d), which was different from that for P-glycoprotein-mediated VCR transport. Our data also suggested that erlotinib has stronger inhibitory activity to BCRP than FTC. Collectively, these results indicated that the inhibitory mechanism of erlotinib on the transporter function of P-glycoprotein seemed different from that on the BCRP function.

Discussion

We have previously shown functional interplay between gefitinib and BCRP[12] which suggested gefitinib as a competitor for other BCRP substrates, including SN-38 and MXR. In the present study, we further demonstrated that erlotinib modulated BCRP-mediated drug resistance and efflux at sub-micromoler concentrations like a competitive inhibitor. Conversely, we found that erlotinib had only minimal effects on P-glycoprotein-mediated drug resistance to MXR and DOX, and even potentiated MXR resistance in K562/MDR cells at concentrations of 0.15–1.5 μmol/L. In addition, we demonstrated that erlotinib restored intracellular accumulation of MXR in BCRP-expressing K562 cells, but did not in P-glycoprotein-expressing K562 cells. Furthermore, we showed that erlotinib selectively inhibited the P-glycoprotein-mediated efflux of VCR by a complicated mechanism, but not that of MXR. These data demonstrate for the first time that the bidirectional modulation of P-glycoprotein-mediated drug resistance by erlotinib is substrate dependent.

P-glycoprotein drug interaction sites are thought to localize to the transmembrane domains, and the presence of multiple drug binding sites has been suggested.[21] Although putative interaction sites for MXR and DOX are not well defined, the mode of interaction for DOX with P-glycoprotein seems to be different from that of *vinca* alkaloids. Specifically, substitution of P-glycoprotein

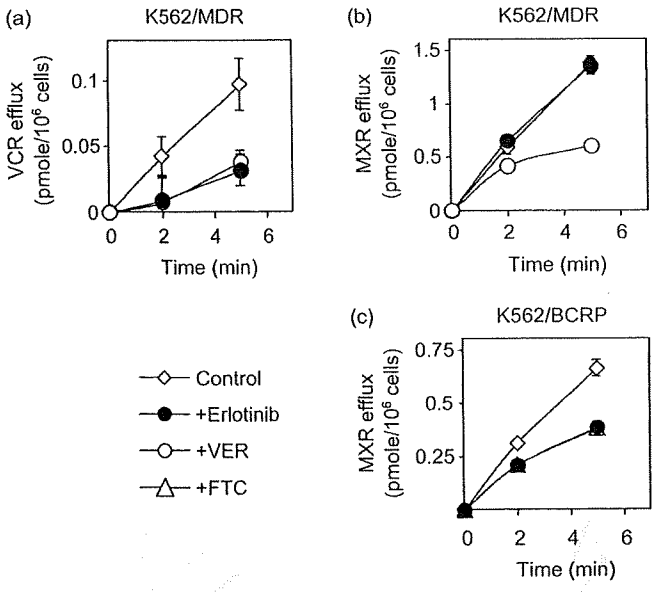

Fig. 5. Effect of erlotinib on the cellular efflux vincristine (VCR) and mitoxantrone (MXR). K562/MDR (a and b) and K562/BCRP (c) cells were pre-treated with ^{3}H-labeled substrates. Erlotinib, verapamil (VER), and fumitremorgin C (FTC) were tested to suppress efflux of incorporated substrate as described in 'Materials and Methods'. The efflux of ^{3}H-labeled substrate was determined by measuring their radioactivity levels released into the culture medium. Data are the means ± SD of triplicate determinations.

Phe-335 in transmembrane domain 6 with alanine resulted in a loss of resistance to vinblastine, but retention of resistance to DOX.[22] The RI50 value of erlotinib for DOX resistance in K562/MDR cells was approximately 10-fold higher than observed for VCR or PTX resistance (Table 2). Therefore, the region of P-glycoprotein that interacts with erlotinib may be distinct from the DOX interaction site. Further molecular studies will be required to properly elucidate the modes of interaction between kinase inhibitors and P-glycoprotein.

With regard to effects on BCRP by TKIs, previous studies have shown that gefitinib binds to ATP-bound BCRP at an as yet undetermined binding site.[23] Shi *et al.* recently reported that erlotinib did not compete with iodoarylazidoprazosin at the substrate-binding sites on BCRP or P-glycoprotein, although erlotinib stimulates the ATPase activity of both proteins.[16] Since P-glycoprotein and BCRP ATPase activities are stimulated by their substrates, and BCRP expression conferred resistance to erlotinib in PC-9 cells, erlotinib may directly interact with an as yet undetermined site in BCRP and P-glycoprotein and function like a substrate. Indeed, recent study suggests erlotinib as a substrate for both P-glycoprotein and BCRP *in vivo* since P-glycoprotein and BCRP significantly affect the oral bioavailability of erlotinib.[24]

Breast cancer resistance protein (BCRP) was more sensitive to the inhibitory effect of erlotinib than P-glycoprotein, since the RI50 values of erlotinib for BCRP were lower than those for P-glycoprotein (Tables 1 and 2). Consistently, Shi *et al.* also showed that the ATPase activity of BCRP was stimulated by lower concentrations of erlotinib than were required for P-glycoprotein.[16] In addition, gefitinib has been shown to have a higher affinity for BCRP than for P-glycoprotein.[25] Collectively, these observations

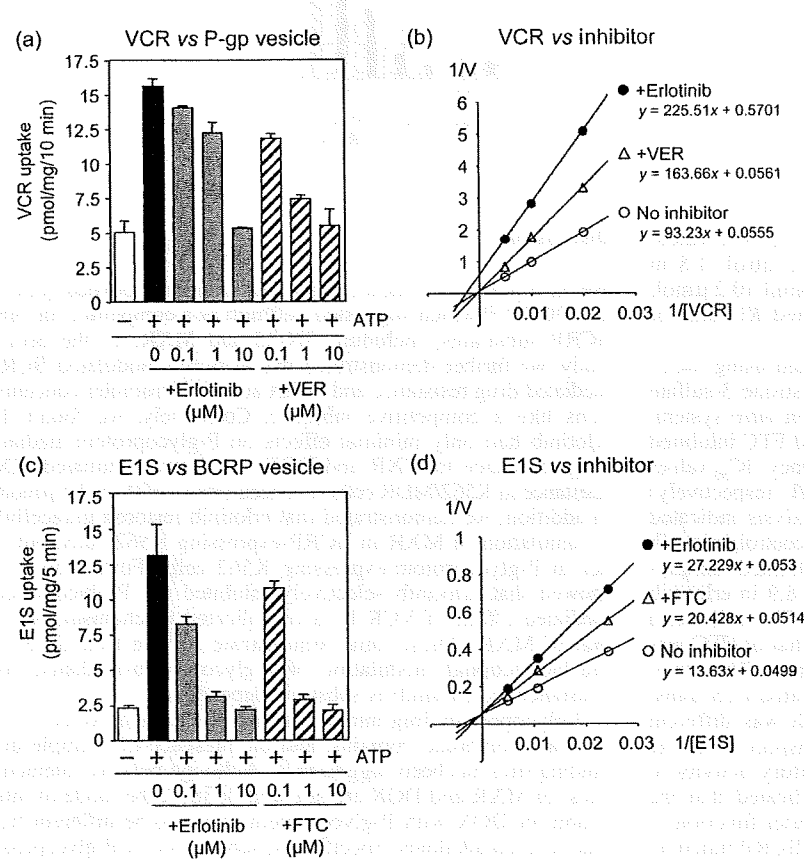

Fig. 6. The intracvesicular transports by P-glycoprotein and breast cancer resistance protein (BCRP) and Lineweaver-Burk plot analysis. Membrane vesicles from K562/MDR (a and b) and from K562/BCRP (c and d) cells were incubated for 10 min with [^{3}H]VCR (a and b) and [^{3}H]E1S (c and d) in the absence or presence of erlotinib, verapamil, or fumitremorgin C (FTC) as described in 'Materials and Methods'. The concentration of ^{3}H-labeled transporter substrate was 100 or 50 nmol/L in the experiments (a) and (c), and those in (c) and (d) were 100, 200, 400 or 50, 100, 200 nmol/L respectively. Erlotinib at 2 μmol/L and verapamil (VER) at 0.2 μmol/L were tested in experiment (c), and erlotinib at 0.13 μmol/L and FTC at 0.25 μmol/L were in experiment (d). The transport of ^{3}H-labeled substrate was determined by measuring their radioactivity levels incorporated into the membrane vesicles. Data shown in (a) and (c) are the means ± SD of triplicate determinations, and data in (b) and (d) are the means of duplicated determinations.

doi: 10.1111/j.1349-7006.2009.01213.x

suggest that erlotinib will have a higher affinity for BCRP than for P-glycoprotein.

Studies of erlotinib pharmacokinetics have shown that plasma concentrations of erlotinib are in the micromoler range in clinical situations.[26] Given that erlotinib-mediated modulation of BCRP and P-glycoprotein function was achieved at submicromoler levels in our experiments, erlotinib administration will likely affect the normal functions of BCRP and P-glycoprotein expressed in digestive organs, the kidney, and the blood–brain barrier.

Erlotinib and other TKIs will likely be tested against various tumor types in combination with chemotherapy, but the benefits of such combination therapy are not yet apparent.[27] Molecular analysis suggests that EGFR-activation mutations found in some patients are correlated with the best outcome in combination therapy with EGFR-TKIs and conventional anticancer drugs.[28] Importantly, our findings demonstrate that the pharmacological effect of erlotinib on P-glycoprotein varies among substrates. Further efforts for the understanding of pharmacological interaction between TKIs and anticancer drugs would be beneficial to improve the effectiveness of combination therapy.[29] These preclinical studies on the TKIs, the ABC transporters, and their substrates would also contribute to prevent the occurrence of unexpected adverse effects when utilizing combinational chemotherapy.

Acknowledgments

This work was supported by Grants-in-Aid from the Ministry of Education, Culture, Sports, Science and Technology; and from the Ministry of Health, Labor and Welfare, Japan. We thank Yuka Shimomura for performing the initial experiments in this work and other laboratory members for their helpful discussions.

Abbreviations

ABC	ATP-binding cassette
ATP	adenosine triphosphate
BCRP	breast cancer resistance protein
EGFR	epidermal growth factor receptor
IC_{50}	50% inhibitory concentration
TKI	tyrosine kinase inhibitor

References

1 Gottesman MM, Fojo T, Bates SE. Multidrug resistance in cancer: role of ATP-dependent transporters. *Nat Rev Cancer* 2002; **2**: 48–58.
2 Sugimoto Y, Tsukahara S, Ishikawa E, Mitsuhashi J. Breast cancer resistance protein: molecular target for anticancer drug resistance and pharmacokinetics/pharmacodynamics. *Cancer Sci* 2005; **96**: 457–65.
3 Doyle LA, Ross DD. Multidrug resistance mediated by the breast cancer resistance protein BCRP (ABCG2). *Oncogene* 2003; **22**: 7340–58.
4 Tsuruo T, Iida H, Tsukagoshi S, Sakurai Y. Overcoming of vincristine resistance in P388 leukemia in vivo and in vitro through enhanced cytotoxicity of vincristine and vinblastine by verapamil. *Cancer Res* 1981; **41**: 1967–72.
5 Fojo T, Bates S. Strategies for reversing drug resistance. *Oncogene* 2003; **22**: 7512–23.
6 Rabindran SK, Ross DD, Doyle LA, Yang W, Greenberger LM. Fumitremorgin C reverses multidrug resistance in cells transfected with the breast cancer resistance protein. *Cancer Res* 2000; **60**: 47–50.
7 Sugimoto Y, Tsukahara S, Imai Y, Ueda K, Tsuruo T. Reversal of breast cancer resistance protein-mediated drug resistance by estrogen antagonists and agonists. *Mol Cancer Ther* 2003; **2**: 105–12.
8 Katayama K, Masuyama K, Yoshioka S, Hasegawa H, Mitsuhashi J, Sugimoto Y. Flavonoids inhibit breast cancer resistance protein-mediated drug resistance: transporter specificity and structure-activity relationship. *Cancer Chemother Pharmacol* 2007; **60**: 789–97.
9 Kumar A, Petri ET, Halmos B, Boggon TJ. Structure and clinical relevance of the epidermal growth factor receptor in human cancer. *J Clin Oncol* 2008; **26**: 1742–51.
10 Harari PM, Allen GW, Bonner JA. Biology of interactions: antiepidermal growth factor receptor agents. *J Clin Oncol* 2007; **25**: 4057–65.
11 Mukai M, Che XF, Furukawa T *et al.* Reversal of the resistance to STI571 in human chronic myelogenous leukemia K562 cells. *Cancer Sci* 2003; **94**: 557–63.
12 Yanase K, Tsukahara S, Asada S, Ishikawa E, Imai Y, Sugimoto Y. Gefitinib reverses breast cancer resistance protein-mediated drug resistance. *Mol Cancer Ther* 2004; **3**: 1119–25.
13 Perez-Soler R. Erlotinib: recent clinical results and ongoing studies in non small cell lung cancer. *Clin Cancer Res* 2007; **13**: s4589–92.
14 Cohen MH, Johnson JR, Chen YF, Sridhara R, Pazdur R. FDA drug approval summary: erlotinib (Tarceva) tablets. *Oncologist* 2005; **10**: 461–6.
15 Moore MJ, Goldstein D, Hamm J *et al.* Erlotinib plus gemcitabine compared with gemcitabine alone in patients with advanced pancreatic cancer: a phase III trial of the National Cancer Institute of Canada Clinical Trials Group. *J Clin Oncol* 2007; **25**: 1960–6.
16 Shi Z, Peng XX, Kim IW *et al.* Erlotinib (Tarceva, OSI-774) antagonizes ATP-binding cassette subfamily B member 1 and ATP-binding cassette subfamily G member 2-mediated drug resistance. *Cancer Res* 2007; **67**: 11012–20.
17 Shi Z, Parmar S, Peng XX *et al.* The epidermal growth factor tyrosine kinase inhibitor AG1478 and erlotinib reverse ABCG2-mediated drug resistance. *Oncol Rep* 2009; **21**: 483–9.
18 Sugimoto Y, Sato S, Tsukahara S *et al.* Coexpression of a multidrug resistance gene (MDR1) and herpes simplex virus thymidine kinase gene in a bicistronic retroviral vector Ha-MDR-IRES-TK allows selective killing of MDR1-transduced human tumors transplanted in nude mice. *Cancer Gene Ther* 1997; **4**: 51–8.
19 Naito M, Hamada H, Tsuruo T. ATP/Mg2+-dependent binding of vincristine to the plasma membrane of multidrug-resistant K562 cells. *J Biol Chem* 1988; **263**: 11887–91.
20 Arao T, Fukumoto H, Takeda M, Tamura T, Saijo N, Nishio K. Small in-frame deletion in the epidermal growth factor receptor as a target for ZD6474. *Cancer Res* 2004; **64**: 9101–4.
21 Loo TW, Clarke DM. Mutational analysis of ABC proteins. *Arch Biochem Biophys* 2008; **476**: 51–64.
22 Loo TW, Clarke DM. Functional consequences of phenylalanine mutations in the predicted transmembrane domain of P-glycoprotein. *J Biol Chem* 1993; **268**: 19965–72.
23 Saito H, Hirano H, Nakagawa H *et al.* A new strategy of high-speed screening and quantitative structure-activity relationship analysis to evaluate human ATP-binding cassette transporter ABCG2-drug interactions. *J Pharmacol Exp Ther* 2006; **317**: 1114–24.
24 Marchetti S, de Vries NA, Buckle T *et al.* Effect of the ATP-binding cassette drug transporters ABCB1, ABCG2, and ABCC2 on erlotinib hydrochloride (Tarceva) disposition in in vitro and in vivo pharmacokinetic studies employing Bcrp1-/-/Mdr1a/1b-/- (triple-knockout) and wild-type mice. *Mol Cancer Ther* 2008; **7**: 2280–7.
25 Ozvegy-Laczka C, Hegedus T, Varady G *et al.* High-affinity interaction of tyrosine kinase inhibitors with the ABCG2 multidrug transporter. *Mol Pharmcol* 2004; **65**: 1485–95.
26 Hamilton M, Wolf JL, Rusk J *et al.* Effects of smoking on the pharmacokinetics of erlotinib. *Clin Cancer Res* 2006; **12**: 2166–71.
27 Herbst RS, Prager D, Hermann R *et al.* TRIBUTE: a phase III trial of erlotinib hydrochloride (OSI-774) combined with carboplatin and paclitaxel chemotherapy in advanced non-small-cell lung cancer. *J Clin Oncol* 2005; **23**: 5892–9.
28 Bonomi PD, Buckingham L, Coon J. Selecting patients for treatment with epidermal growth factor tyrosine kinase inhibitors. *Clin Cancer Res* 2007; **13**: s4606–12.
29 Milano G, Spano JP, Leyland-Jones B. EGFR-targeting drugs in combination with cytotoxic agents: from bench to bedside, a contrasted reality. *Br J Cancer* 2008; **99**: 1–5.

Acyl-CoA synthetase as a cancer survival factor: its inhibition enhances the efficacy of etoposide

Tetsuo Mashima,[1] Shigeo Sato,[2] Sachiko Okabe,[1] Satoshi Miyata,[3] Masaaki Matsuura,[3,4] Yoshikazu Sugimoto,[5,6] Takashi Tsuruo[7,8] and Hiroyuki Seimiya[1,9]

[1]Divisions of Molecular Biotherapy, [2]Experimental Chemotherapy, Cancer Chemotherapy Center, [3]Genome Center, [4]Division of Cancer Genomics, The Cancer Institute, Japanese Foundation for Cancer Research, Koto-ku, Tokyo; [5]Department of Chemotherapy, Faculty of Pharmacy, Keio University, Minato-ku, Tokyo; [6]Division of Gene Therapy, [7]Director's Room, Cancer Chemotherapy Center, Japanese Foundation for Cancer Research, Koto-ku, Tokyo, Japan

(Received March 26, 2009/Revised April 24, 2009/Accepted April 24, 2009/Online publication May 13, 2009)

Lipid metabolism is often elevated in cancer cells and plays an important role in their growth and malignancy. Acyl-CoA synthetase (ACS), which converts long-chain fatty acids to acyl-CoA, is overexpressed in various types of cancer. However, the role of ACS in cancer remains unknown. Here, we found that ACS enzyme activity is required for cancer cell survival. Namely, the ACS inhibitor Triacsin c induced massive apoptosis in glioma cells while this cell death was completely suppressed by overexpression of ACSL5, the Triacsin c–resistant ACS isozyme, but not by overexpression of a catalytically inactive ACSL5 mutant. ACS inhibition by Triacsin c markedly potentiated the Bax-induced intrinsic apoptotic pathway by promoting cytochrome c release and subsequent caspase activation. These effects were abrogated by ACSL5 overexpression. Correspondingly, ACS inhibition synergistically potentiated the glioma cell death induced by etoposide, a well-known activator of apoptosis. Furthermore, in a nude mouse xenograft model, Triacsin c at a non-toxic dose enhanced the antitumor efficacy of a low-dose chemotherapy with etoposide. These results indicate that ACS is an apoptosis suppressor and that ACS inhibition could be a rational strategy to amplify the antitumor effect of etoposide. (*Cancer Sci* 2009; 100: 1556–1562)

Overexpression of lipogenic enzymes is a common characteristic of many cancers.[1] In tumor cells, the supply of cellular fatty acids is highly dependent on de novo biosynthesis. FASN is a key enzyme that catalyzes the terminal step in the *de novo* synthesis of saturated fatty acids. Fatty acid synthase (FASN) is overexpressed in a wide variety of human epithelial cancer cells and plays a critical role in tumor growth and survival.[2] In addition to FASN, several other enzymes involved in lipid metabolism have recently been shown to be involved in tumor growth and malignancy.[3,4] These observations support the notion that elevated lipid metabolism could be a rational target for cancer treatment.

Acyl-CoA synthetases (ACS) are enzymes that act downstream of FASN and convert long-chain fatty acids to acyl-CoA.[5] This reaction is a crucial step in several lipid metabolism pathways, including phospholipid biosynthesis, lipid modification of cellular proteins, and β-oxidation. In mammals, five ACS isozymes have been identified. Previous reports have indicated that several ACS isozymes, such as ACSL4 and ACSL5, are overexpressed in cancer cells.[6–9] We recently identified Triacsin c, a potent inhibitor of ACS, as an agent that shows selective cytotoxicity to malignant cancer cells.[10] These observations suggest that ACS could play a predominant role in cancer cell survival. Still, however, it remains unclear how ACS regulates cell death and whether the ACS inhibition could affect the chemosensitivity of cancer.

Activation of apoptotic pathways is a key mechanism by which anticancer agents kill tumor cells.[11] Chemotherapeutic agents induce apoptosis through the intrinsic mitochondria-dependent pathway that is activated mainly by the release of cytochrome c from the mitochondria. The released cytochrome c interacts with Apaf-1 to form an Apaf-1 multimer (apoptosome), which in turn activates caspase-9 and the downstream caspases that participate in the execution phase of apoptosis.[12] The activated caspases cleave many kinds of substrates, leading to cell death. Several factors, e.g. Bcl-2 family members, suppress apoptosis on the mitochondria.[13] Because these antiapoptotic factors are frequently overexpressed in cancer cells and are involved in chemotherapy resistance, trials have been undertaken to identify their specific inhibitors, some of which are now being tested clinically.[14–16]

In the present study, we examined the antiapoptotic role of ACS in cancer cells. We found that ACS enzyme activity was essential for glioma cell survival. Moreover, we demonstrate the combinational effect of ACS inhibition with etoposide.

Materials and Methods

Chemicals. Triacsin c was purchased from Sigma (St. Louis, MO, USA). Etoposide was purchased from Bristol-Myers Squibb (New York, NY, USA). Caspase inhibitor Z-VAD-fmk and caspase substrate peptide DEVD-MCA were purchased from Peptide Institute (Osaka, Japan).

Cell culture, detection of apoptotic cells, and measurement of cell growth. Human glioma SF268 and U251 cells were cultured in RPMI-1640 supplemented with 10% heat-inactivated fetal bovine serum and 100 μg/mL kanamycin in a humidified atmosphere of 5% CO_2 and 95% air. Drug sensitivity was evaluated using the MTS method.[17] In brief, we used a CellTiter 96AQ$_{ueous}$ One Solution Cell Proliferation Assay Kit (Promega, Tokyo, Japan). Twenty microliters of MTS and phenazine ethosulfate solution were added to the drug-treated cells (100 μL/well in 96-well plates) and the mixture was incubated at 37°C for 30–60 min. For quantitation of relative cell number, OD490 was measured using a microplate reader. To detect apoptotic cells, cell nuclei were stained with Hoechst 33342.[18] Apoptotic cells were evaluated using such characteristic nuclear features as chromatin condensation and nuclear fragmentation.

Caspase and apoptosome assays. Cell lysates were prepared and caspase activity was measured using DEVD-MCA as a substrate, as described previously.[17] To estimate Bax-induced caspase activation, we transfected cells with pCGBL-HA-Bax and pGVC, a luciferase-expressing construct driven by a SV40 promoter and enhancer.[18] After transfection and subsequent drug treatment, cell lysates were prepared and caspase activity was measured. To monitor the transfection efficiency, we also measured luciferase activities in cell lysates using the Luciferase Assay System (Promega). The caspase activity was normalized by the luciferase

[8]Deceased.

[9]To whom correspondence should be addressed. E-mail: hseimiya@jfcr.or.jp

doi: 10.1111/j.1349-7006.2009.01203.x

activity to estimate relative Bax-dependent caspase activation. To measure apoptosome activity, cytosolic extracts were prepared as described previously[17] and incubated with 10 μM cytochrome c and 1 mM dATP for 20–40 min. After the incubation, caspase activity was measured.

Subcellular fractionation and western blot analysis. Subcellular fractions were obtained by using a ProteoExtract Subcellular Proteome Extraction kit (Calbiochem, San Diego, CA, USA). Each extract derived from the same number of the cells was subjected to SDS-PAGE. To analyze apoptosis regulators' expression, we washed cells in ice-cold phosphate-buffered saline (PBS) and lyzed them in TNE buffer (10 mM Tris-HCl [pH 7.8], 1% Nonidet P-40, 150 mM NaCl, 1 mM EDTA, and 10 μg/mL aprotinin) on ice for 30 min. After centrifugation at 12 000*g* for 10 min at 4°C, the supernatant (TNE lysate) was subjected to SDS-PAGE. For detection of cytochrome c release from the mitochondria, cytosolic extracts were prepared as described previously[10] and were subjected to SDS-PAGE. Western blot analysis was performed as described previously[19] with the following primary antibodies: mouse anti-FLAG (M2; Sigma), mouse anti-PARP (BD Pharmingen, San Diego, CA, USA), rabbit anti-EGFR (Cell Signaling Technology, Beverly, MA, USA), mouse anti-voltage-dependent anion channel (VDAC) (Ab-4; Calbiochem), mouse anti-cytochrome c (7H8.2C12; BD Pharmingen), rabbit anti-HA (Y-11; Santa Cruz Biotechnology, Santa Cruz, CA, USA) mouse anti-α-tubulin (B5-1-2; Sigma), mouse anti-Bcl-2 (BD Pharmingen), mouse anti-Bcl-XL (BD Pharmingen), or mouse anti-Bax (BD Pharmingen).

Immunofluorescence staining. Cells were fixed with 2% paraformaldehyde/PBS and permeabilized with 0.5% NP40/PBS. The fixed cells were blocked in PBS containing 1% bovine serum albumin and incubated with rabbit anti-FLAG (Sigma) and mouse anti-cytochrome c (6H2.B4; BD Pharmingen) antibodies. These primary antibodies were detected with Rhodamine-conjugated anti-rabbit Ig and FITC-conjugated anti-mouse Ig, respectively. DNA was stained with 0.2 μg/mL of DAPI. Images were acquired using an Olympus IX-71 microscope with a DP70 digital camera and Lumina Vision software (Mitani Corporation, Tokyo, Japan).

Vector construction. For the expression of human ACSL5 and its inactive mutant ACSL5-MT, pHa-ACSL5-FLAG-IRES-DHFR and pHa-ACSL5-MT-FLAG-IRES-DHFR were constructed as described previously.[10,20] To construct an ACSL5 mutant, delta L, that lacked an amino-terminus sequence (amino acid 2–41), we amplified, by polymerase chain reaction (PCR), the ACSL5 fragment that lacked amino acids 2–41 and subcloned it into the pHa vector to generate pHa-ACSL5 (delta L)-FLAG-IRES-DHFR. The full-length cDNA for human Bax was amplified by PCR and subcloned into a pCGBL mammalian expression vector with an N-terminal HA epitope tag to generate pCGBL-HA-Bax.

Transient transfection and retroviral infection. Transient transfection of pCGBL-HA-Bax was performed using Lipofectamine 2000 (Invitrogen, San Diego, CA, USA). For retroviral gene transfer, PA317 cells were transfected with pHa-IRES-DHFR (mock), pHa-ACSL5-FLAG-IRES-DHFR, or ACSL5 mutant constructs, selected with methotrexate (MTX), and culture supernatants of the MTX-resistant PA317 cells were added to SF268 cells, as described previously.[10] After retroviral infection and subsequent methotrexate selection (100 ng/mL), stably transduced cells were established.

Acyl-CoA synthetase (ACS) enzyme assay. Total cell lysates were prepared by homogenizing cells in buffer A, and the ACS activity was measured, as described previously.[10] In brief, the assay mixture contained 1.2 μM $MgCl_2$, 5 μM ATP, 3 μM potassium fluoride, 0.1 μM coenzyme A, 3 μM 2-mercaptoethanol, and 0.03 μM palmitic acid with 0.1 μCi of [^{14}C]-palmitic acid in a total volume of 20 μL. The reaction was initiated by adding 10 μL of cell lysates at 37°C and terminated after 1 h by adding 270 μL of isopropanol-heptane-aqueous 1 M H_2SO_4 (40:10:1 by volume). Then 180 μL of heptane and 120 μL of water were added and the upper layer was discarded. The lower layer was washed twice with 200 μL of heptane containing 15 mM palmitic acid and the radioactivity in 100 μL of the sample was counted in 1 mL of ACS II (Amersham, Tokyo, Japan).

Mouse xenograft therapeutic model. U251 cells (5×10^6 cells/mouse) were implanted subcutaneously in the right flanks of 6-week-old CAnN.Cg-Foxn1nμ/CrlCrlj nude mice (Charles River Laboratories Japan, Kanagawa, Japan). Therapeutic experiments (five mice per group) were started approximately 20 days after implant when tumors reached 90–170 mm^3, as measured with calipers (day 0). Etoposide (12 mg/kg/day) was administered i.v. on days 0, 1, and 2. Triacsin c (4 mg/kg/day) was administered by intratumoral injection in 40 μL of saline on days 0, 1, and 2. Control mice received the same volume of saline as the experimental mice. The length (L) and width (W) of the tumor mass were measured, and the tumor volume (TV) was calculated as: $TV = (L \times W^2)/2$. The difference in the growth rate between etoposide-treated and the etoposide + Triacsin c–treated groups was tested by an autoregressive random errors model[21] using statistical software R[22] (version 2.7.1) with the agce package (version 1.2; http://www.R-project.org). All animal procedures were performed in the animal experiment room of the Japanese Foundation for Cancer Research (JFCR) using protocols approved by the JFCR Animal Care and Use Committee.

Results

Acyl-CoA synthetase (ACS) activity contributes to cancer cell survival. We have shown that Triacsin c, a specific inhibitor of ACS, induces cell death preferentially in tumor cells, but is less toxic to non-cancerous cells.[10] To confirm the requirement for ACS enzyme activity in cancer cell survival, we established cell lines that stably overexpressed either ACSL5 or its inactive mutant (ACSL5-MT), since ACSL5 is a Triacsin c–resistant isozyme among five ACS members,[23] and we postulated that the overexpression of ACSL5 could effectively reverse the inhibition of ACS activity by Triacsin c. We chose glioma cell lines for this experiment since ACSL5 is frequently overexpressed in malignant glioma.[7] When retrovirally transduced in human glioma SF268 cells, wild-type ACSL5 and the ACSL5-MT proteins were stably expressed (Fig. 1a, inset). On the other hand, the ACS activity was exclusively increased in the wild-type ACSL5-expressed cells but not in ACSL5-MT-expressed cells under both Triacsin c–treated and –untreated conditions (Fig. 1a). Triacsin c inhibition of ACS activity was eliminated by wild-type ACSL5 but not by ACSL5-MT. These data indicate that ACSL5-MT acts as an inactive mutant and that these systems work to determine the role of ACS activity in cancer cell survival. We examined the effect of wild-type ACSL5 and ACSL5-MT on Triacsin c–induced SF268 cell death. As shown in Fig. 1(b,c), Triacsin c (3 μM) strongly induced apoptosis and activated caspases in mock cells. Wild-type ACSL5, which retained ACS activity in Triacsin c–treated cells, completely inhibited the caspase activation and apoptotic cell death, while ACSL5-MT did not (Fig. 1b–d). Triacsin c–induced cell death would depend on caspase activation because a caspase inhibitor, Z-VAD-fmk, restored the viable cell number (Fig. 1d). These results indicate that ACS plays an essential role in SF268 cell survival, and that ACS inhibition induces apoptosis of the cells.

Role of subcellular ACS in cancer cell survival. As shown above, ACSL5 overexpression compensated for the decrease of ACS activity in Triacsin c–treated cells and suppressed Triacsin c–induced cell death. Since rat ACSL5 is expressed predominantly on the mitochondrial membrane,[24] we speculated that human ACSL5 could also be expressed on the organelle and would compensate for Triacsin c–induced loss of the ACS activity, leading to cell death suppression. To test this hypothesis, we first examined the subcellular localization of human ACSL5 by immunofluorescence staining (Fig. 2a). Consistent with the

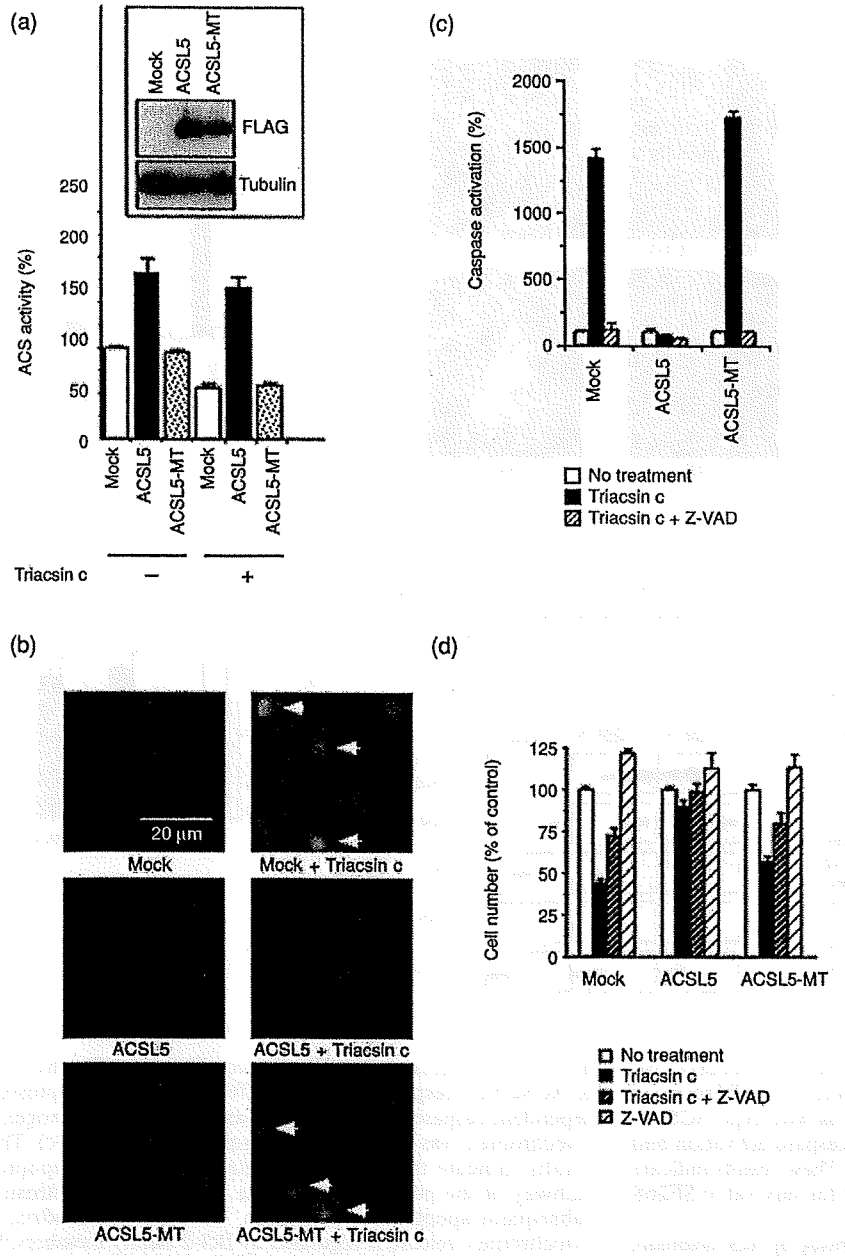

Fig. 1. Acyl-CoA synthetase (ACS) catalytic activity requirement for glioma cell survival. (a) Effect of 48-h Triacsin c treatment (3 μM) on ACS activity in mock-, ACSL5-, and ACSL5-MT–transduced SF268 cells. ACS activity was measured as described in 'Materials and Methods'. Inset, The expressions of ACSL5 and ACSL5-MT were examined by western blot with anti-FLAG M2 antibody. The expression of α-tubulin was analyzed as a loading control. (b) Apoptosis induction after Triacsin c treatment. Cells were treated as in (a). The cell nuclei were stained with Hoechst 33342. Induction of apoptosis in each cell was evaluated using the characteristic nuclear features of apoptosis, such as chromatin condensation and nuclear fragmentation. Arrows indicate apoptotic cells. (c) Caspase activation after Triacsin c treatment. Cells were left untreated or treated with 3-μM Triacsin c in the absence or the presence of 50-μM caspase inhibitor, Z-Val-Ala-Asp(OMe)-CH2F (Z-VAD), for 30 h. Caspase activity was measured as described in 'Materials and Methods'. (d) Cell number after Triacsin c treatment. Cells were treated as in (c) for 48 h and relative cell number was measured using the 3-(4,5-dimethylthiazol-2-yl)-5-(3-carboxymethoxyphenyl)-2-(4-sulfophenyl)-2H-tetrazolium (MTS) method, as described in 'Materials and Methods'. Data are mean values of three independent experiments. Error bars show standard deviations.

previous report of rat ACSL5, human ACSL5 was colocalized with cytochrome c, a marker protein of mitochondria. Furthermore, the patterns of immunofluorescence staining suggested that the human ACSL5 was localized not only to the mitochondria but could also exist at the perinuclear region and, to a lesser extent, in the nucleoplasm (Fig. 2a). To determine the localization of human ACSL5 further, we performed subcellular fractionation of cellular proteins. As shown in Fig. 2(b), ACSL5 was not only present in the organelle/membrane fraction (O/M), which contained mitochondria, but also in the nuclear fraction (N). These data confirmed that ACSL5 was localized in the nuclei of cancer cells as well as to the mitochondria. To clarify the importance of subcellular ACS in SF268 cell survival, we generated deletion mutants of ACSL5 and examined their subcellular localizations. We found that the mutant delta L (Fig. 2b) exclusively lost its nuclear localization, although the amino-terminus sequence that the mutant lacked did not contain any nuclear localization sequence (data not shown, searched by the PSORT II prediction algorithm at http://psort.ims.u-tokyo.ac.jp/form2.html). On the other hand, this mutant still retained the organelle localization and ACS activity. When retrovirally transduced in SF268 cells, both wild-type ACSL5 and the delta L proteins were stably expressed, and, as in the wild-type ACSL5-expressed cells, ACS activity clearly increased in the delta L–expressed cells (Suppl. Fig. 1). These results indicated that the delta L was catalytically active. While the wild-type ACSL5 was detected in both the organelle/membrane and the nuclear fractions, the delta L mutant lost its nuclear localization and instead was included in the organelle/membrane and the cytosol (C) fractions (Fig. 2b). Immunofluorescence staining further revealed that the delta L was still localized to the mitochondria (Suppl. Fig. 2). These data indicate that the N-terminal region deleted in the delta L mutant is required for

doi: 10.1111/j.1349-7006.2009.01203.x

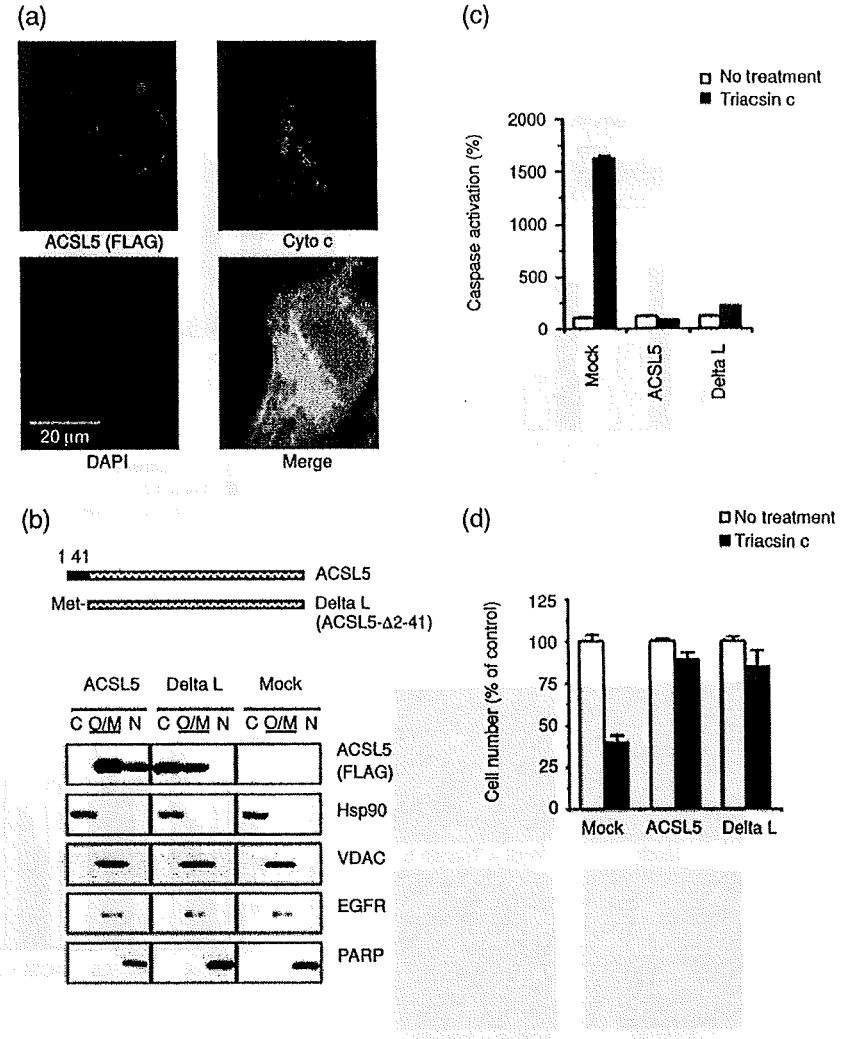

Fig. 2. Organelle-localized acyl-CoA synthetase (ACS) is critical for cancer cell survival. (a) Localization of human ACSL5 in SF268 cells. ACSL5 (FLAG) and the mitochondria marker cytochrome c (Cyto c) were detected by indirect immunofluorescence stain of ACSL5-transduced SF268 cells with anti-FLAG M2 (red) and anti-cytochrome c (green) antibodies, respectively. DAPI staining of DNA is shown in blue. (b) Subcellular fractionation of ACSL5 and its N-terminal deletion mutant (delta L) in SF268 cells. Cytoplasmic (C), organelle/membrane (O/M), and nuclear (N) fractions were prepared, and subjected to western blot analysis with the indicated primary antibodies. Blots with anti-FLAG M2 antibody (FLAG) indicate the expression of ACLS5. Blots with anti-Heat shock protein (Hsp)-90, voltage-dependent anion channel (VDAC), epidermal growth factor receptor (EGFR), and poly(ADP-ribose) polymerase (PARP) antibodies demonstrate the purity of their respective fractions. (c) Caspase activation in SF268/ACSL5 and SF268/delta L cells after Triacsin c treatment. Mock-, ACSL5-, and delta L-transduced SF268 cells were left untreated or treated with 3-μM Triacsin c for 30 h. Caspase activity was measured as described in 'Materials and Methods'. (d) Cell number after Triacsin c treatment. Cells were treated as in (c) for 48 h and relative cell number was measured using the 3-(4,5-dimethylthiazol-2-yl)-5-(3-carboxymethoxyphenyl)-2-(4-sulfophenyl)-2H-tetrazolium (MTS) method. In (c) and (d), data are mean values of three independent experiments, and error bars show standard deviations.

ACSL5 targeting to the nuclei but not to the mitochondria. We compared the effect of ACSL5 and the delta L on Triacsin c–induced cell death and found that, as well as wild-type ACSL5, the delta L mutant efficiently suppressed caspase activation and cell death caused by Triacsin c (Fig. 2c,d). These results indicate that the nuclear ACS could not be required for survival of SF268 cells.

Enhancement of the intrinsic apoptosis pathway by ACS inhibition. To determine the role of ACS in glioma cell survival, we examined whether ACS could act as a repressor against mitochondria-dependent apoptosis. Mitochondrial apoptosis inducers, such as Bax protein, can directly activate this intrinsic apoptosis pathway.[25,26] Therefore, we tested the effect of ACS inhibition on Bax-induced apoptosis. As shown in Figure 3(a), Bax activated caspases in a dose-dependent manner. Sublethal dose of Triacsin c potentiated this Bax-induced caspase activation. Moreover, this effect was strongly suppressed by compensation of ACS activity by ACSL5 overexpression. These results indicate the antagonistic role of ACS in the mitochondrial apoptosis pathway, and ACS inhibition potentiates this pathway. To clarify the molecular mechanisms further, we examined the effect of ACS inhibition on Bax-induced cytochrome c release from the mitochondria to cytoplasm. When cells were expressed with Bax alone, cytochrome c release to the cytosol was below detection levels in western blot analysis. On the other hand, we found that the cytochrome c release was clearly enhanced by Triacsin c, which was suppressed by ACSL5 expression (Fig. 3b). By contrast, Triacsin c treatment or ACSL5 overexpression did not affect the *in vitro* apoptosome-dependent caspase activation that was initiated when exogenous cytochrome c was added to the cytosolic extracts (Fig. 3c). These results indicate that ACS antagonizes the intrinsic apoptosis pathway at the point of cytochrome c release and upstream of subsequent apoptosome activation. On the mitochondria, the cytochrome c release is regulated by Bcl-2 family members.[13,15] So next, we examined the effect of ACS inhibition on the protein expression of the apoptosis regulators in mock and ACSL5-overexpressed cells. We found that ACS inhibition did not affect protein levels of the mitochondrial Bcl-2 family members, Bcl-2, Bcl-XL, and Bax (Suppl. Fig. 3), suggesting the involvement of other factors in the apoptosis enhancement.

Potentiation of etoposide-induced cell death by ACS inhibition. Because ACS inhibition potentiated activation of the intrinsic apoptosis pathway, we examined whether ACS inhibition also enhances chemotherapeutic agent–induced death of cancer cells. We initially examined combinations of several chemotherapeutic drugs with Triacsin c, and determined the optical conditions for maximal efficacy. As a result, we found the synergistic effect of ACS inhibition with etoposide. As a result, we found the combinational effect of Triacsin c with etoposide, which induces apoptosis through the mitochondria-mediated pathway.[27,28] When SF268/mock cells were treated with either etoposide (0.3 μg/mL, 48 h) or a sublethal dose of Triacsin c (1 μM, 48 h), caspases were

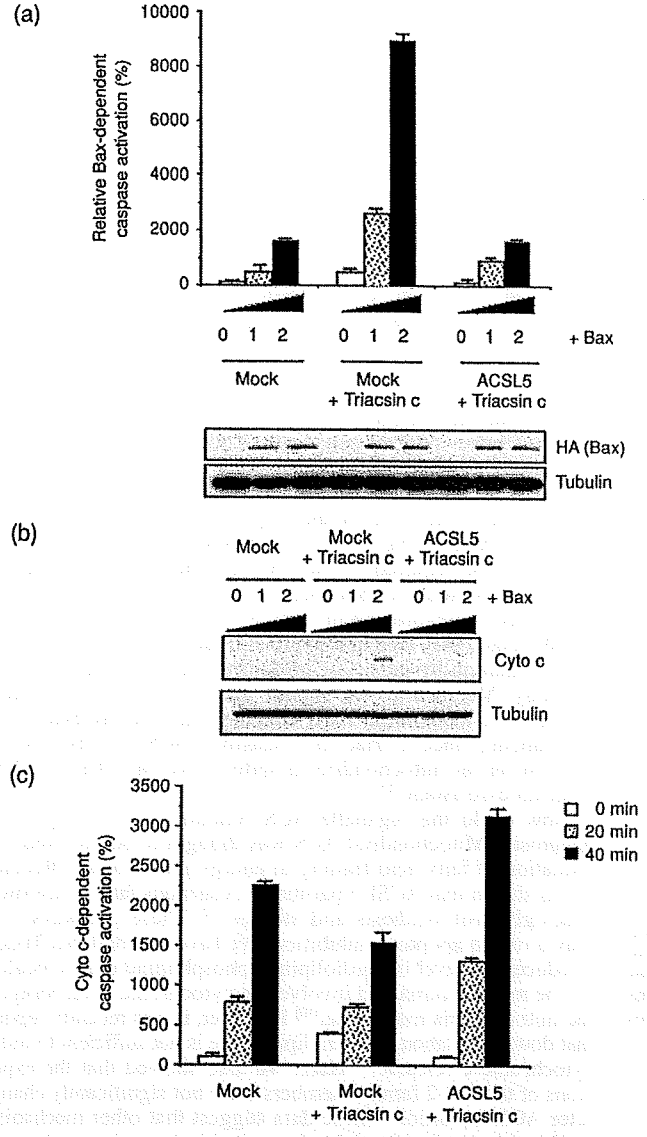

Fig. 3. Potentiating the mitochondrial apoptosis pathway by acyl-CoA synthetase (ACS) inhibition. (a) To estimate Bax-induced caspase activation, mock- and ACSL5-transduced SF268 cells were seeded in six-well plates and transiently transfected with pCGBL-HA-Bax (0, 0.1, and 0.2 μg/well) and pGVC, a luciferase-expressing construct (0.4 μg/well). At 6 h after transfection, cells were left untreated or were treated with 1 μM Triacsin c for an additional 24 h. Each cell lysate was prepared and caspase activity measured as described in 'Materials and Methods'. The expression of Bax (HA) was examined by western blot. The expression of α-tubulin was analyzed as a loading control. (b) Cells were transiently transfected with the Bax plasmid vector and then were treated with Triacsin c as in (a). Cytochrome c release from the mitochondria to cytoplasm was monitored by western blot analysis. (c) Mock- and ACSL5-transduced SF268 cells were left untreated or treated with 1 μM Triacsin c for 24 h. Cytosolic extracts were prepared and incubated with 10 μM cytochrome c and 1 mM dATP for 0–40 min. After the incubation, caspase activity was measured, as described in 'Materials and Methods'. In (a) and (c), data are mean values of three independent experiments. Error bars show standard deviations.

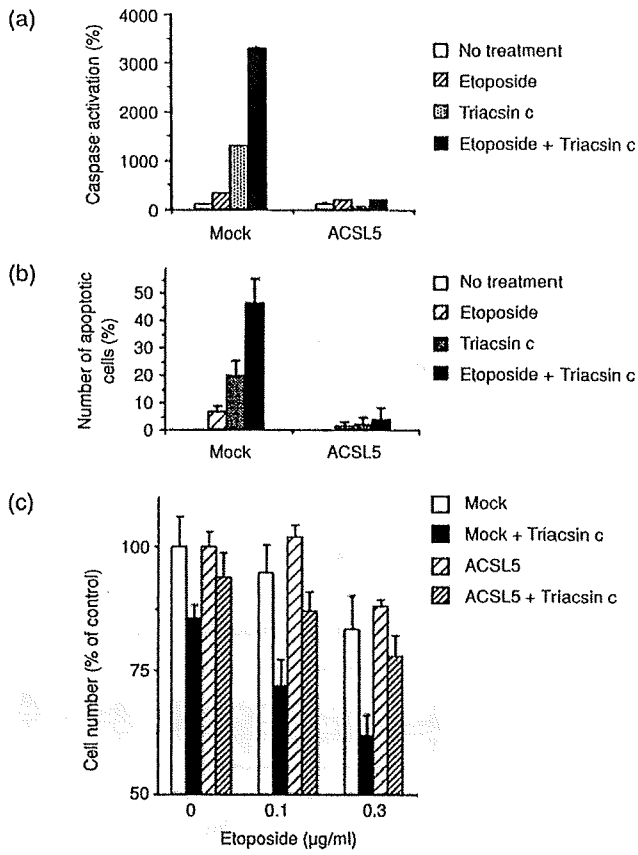

Fig. 4. Potentiating etoposide-induced cell death by acyl-CoA synthetase (ACS) inhibition. (a) Enhanced activation of caspase by etoposide in combination with Triacsin c. Mock- and ACSL5-transduced SF268 cells were left untreated or were treated with 0.3 μg/mL of etoposide, 1 μM Triacsin c or 0.3 μg/mL of etoposide and 1 μM Triacsin c for 48 h. Caspase activity was measured as described in 'Materials and Methods'. (b) Potentiation of apoptosis by etoposide in combination with Triacsin c. Mock- and ACSL5-transduced SF268 cells were treated as in (a), and apoptotic cells were evaluated and counted. (c) Effect of ACS inhibition on etoposide-induced cytotoxicity. Mock- and ACSL5-transduced SF268 cells were left untreated or were treated with the indicated concentrations of etoposide in the absence or presence of 1 μM Triacsin c for 48 h. Cell viability was measured, using the 3-(4,5-dimethylthiazol-2-yl)-5-(3-carboxymethoxyphenyl)-2-(4-sulfophenyl)-2H-tetrazolium (MTS) method. Data are mean values of three independent experiments. Error bars show standard deviations.

activated 3.5-fold or 13-fold, respectively, compared to non-treated cells (Fig. 4a). Co-treatment with etopiside and Triacsin c significantly enhanced the caspase activation (33-fold). This synergism in caspase activation by etoposide and Triacsin c was quenched by ACSL5 overexpression. Correspondingly, the sublethal dose of Triacsin c (1 μM) significantly potentiated etoposide-induced apoptosis (Fig. 4b) and the loss of cell numbers (Fig. 4c). Again, these effects of Triacsin c were canceled by ACSL5 overexpression. These results indicate that inhibiting ACS activity would be a rational strategy to potentiate etoposide-induced cytotoxicity.

To test whether ACS inhibition could increase the antitumor efficacy of etoposide, we developed a tumor xenograft model in nude mice. Because SF268 cells could not form stable tumors in nude mice (our unpublished observation), we chose another implantable glioma cell line, U251, for this *in vivo* study. Mice were treated with saline (control), etoposide, Triacsin c, or etoposide in combination with Triacsin c. Under the limited dose conditions in Figure 5(a), etoposide or Triacsin c alone did not show apparent antitumor effects. Strikingly, however, cotreatment with etoposide and Triacsin c significantly retarded tumor growth. During the treatment, no toxic death or significant body weight change was observed (Fig. 5b). These results indicate

doi: 10.1111/j.1349-7006.2009.01203.x

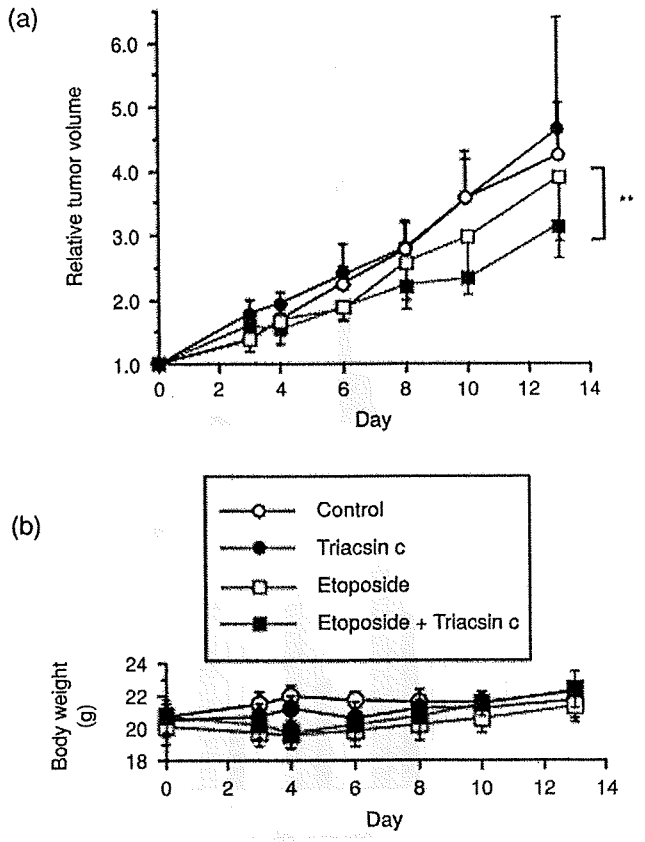

Fig. 5. Triacsin c enhances the efficacy of etoposide *in vivo*. Therapeutic experiments (five mice per group) were started (day 0) when U251 tumors reached 90–170 mm³. Etoposide (12 mg/kg/day) was administrated i.v. on days 0, 1, and 2. Triacsin c (4 mg/kg/day) was administrated by intratumoral injection in 40 μL of saline on days 0, 1, and 2. Control mice received the same volume of saline. Relative tumor volumes and body weight changes of the mice are shown in (a) and (b), respectively. Data are mean values for five mice, and error bars show standard deviations. Statistical evaluations were performed as described in 'Materials and Methods'. $^{**}P < 0.01$.

that the ACS inhibition potentiates the antitumor effect of etoposide *in vivo* with minimal side effects in the mice.

Discussion

ACS catalyzes a critical step in both the anabolic and catabolic pathways of fatty acid metabolism. In our present study, we showed that ACS enzyme activity is a critical factor for cancer cell survival and apoptosis inhibition. When cancer develops, excessive mitogenic signals, due to oncogenic activation or uncontrolled cell cycle progression, are coupled with constitutive activation of the intrinsic apoptosis machinery.[29] Under these conditions, expressions of antiapoptotic factors are requisite for cancer cell survival, and these factors could be the cells' Achilles heel. In fact, agents or strategies that suppress antiapoptotic proteins or directly activate the mitochondria-dependent apoptosis pathway (apoptosome pathway) selectively induce tumor cell death or potentiate the chemosensitivity of tumor cells.[13,14,16,30,31] Our present results suggest that ACS could be one such factor essential for cancer cell survival and whose inhibition induces tumor-selective cell death.

ACS inhibition potentiated Bax- and etoposide-induced apoptosis (Figs 3 and 4). Consistently, the overexpression of ACSL5 suppressed apoptosis induced by etoposide (Fig. 4a,b). These data indicate that ACS could act as an apoptosis inhibitor in tumor cells.

We have shown that ACSL5 nearly completely suppressed Triacsin c–induced cell death. Since small molecules could have off-targets, we cannot exclude the possibility of an ACS-unrelated, off-target effect of Triacsin c. However, such effect would be minor, if any, in our experimental settings, because the catalytically inactive ACSL5 mutant did not suppress the Triacsin c–induced cell death. Thus, Triacsin c could induce apoptosis mainly through ACS inhibition. Meanwhile, because ACS have five isoforms, it is difficult to perform gene-knockdown experiments or to examine the effect of dominant-negative mutants.

ACS shows various subcellular localizations.[24] The ACS inhibitor–induced apoptosis was suppressed by ACSL5, which localizes on the mitochondria and in the nuclei. Moreover, the ACSL5 mutant lacking nuclear localization still inhibited the ACS inhibitor–induced cell death. These data indicate that the nuclear ACS is not required for cancer cell survival and suggest that the organelle ACS could be a critical factor for the survival. To be sure of the role of the organelle ACS, however, further studies with an ACSL5 mutant that lacks the organelle localization could be required. Given the fact that ACSL5 is the only known ACS isozyme that localizes to the mitochondria and is frequently overexpressed in human cancers, it is suggested that ACSL5 could play an important role in tumorigenesis or malignant transformation by means of inhibiting mitochondrial apoptosis pathway. Meanwhile, we should take into account additional unknown mitochondrial ACS enzymes that are involved in this mechanism, since a Triacsin c–sensitive ACS activity is known to exist on rat mitochondria in spite of the fact that ACSL5 is Triacsin c–resistant.[23]

How could the organelle ACS function as an antagonist of apoptosis? Mitochondrial ACS was thought to be involved in β-oxidation of fatty acid leading to energy production.[5] Recently, it was shown that ACSL5 partitions exogenous fatty acids toward triacylglycerol synthesis and storage.[32] These pathways could play a role in apoptosis inhibition. We have reported that Triacsin c reduces the level of cardiolipin, a phospholipid that is localized on the mitochondria and involved in cytochrome c anchorage on the mitochondria membrane.[10] However, it was recently reported that down-regulation of cardiolipin alone is not sufficient to induce cytochrome c release.[33] Here, we also showed that the expressions of the Bcl-2 family members were not significantly changed after ACS inhibition. These data suggest that other mechanisms could also be involved in the potentiation of cytochrome c release by ACS inhibition.

In the present study, we demonstrated that ACS inhibition enhances the etoposide-induced cell death of human glioma cells. We examined combinations of several agents with Triacsin c and also found a synergistic effect of the ACS inhibitor with SN-38 (data not shown). Lipid metabolism is selectively activated in a wide variety of cancers, and ACS is overexpressed in such cancers as glioma, colon cancer, and hepatocellular cancer.[7–9,34] Our data suggest that ACS inhibition would be a rational strategy to potentiate chemosensitivity of cancer. Additional studies, including the combinational effect of ACS inhibition with other antitumor agents, could further clarify the importance of ACS as a new therapeutic target for cancer.

Acknowledgments

We thank the National Cancer Institute as well as Takao Yamori for providing us human glioma cell lines. We also thank members in our laboratory for helpful discussions. This work was supported by grants-in-aid for Cancer Research on Priority Areas (T. Mashima, T. Tsuruo, H. Seimiya) and Young Scientists (T. Mashima) from the Ministry of Education, Culture, Sports, Science and Technology, Japan.

Abbreviations

ACS	Acyl-CoA synthetase
DAPI	4,6-diamino-2-phenylindole
DEVD-MCA	Acetyl-Asp-Glu-Val-Asp-(4-methyl-coumaryl-7-amide)
EGFR	Epidermal growth factor receptor
FASN	Fatty acid synthase
Hsp	Heat shock protein
MTS	3-(4,5-dimethylthiazol-2-yl)-5-(3-carboxymethoxyphenyl)-2-(4-sulfophenyl)-2H-tetrazolium
PARP	Poly(ADP-ribose) polymerase
Z-VAD-fmk	Z-Val-Ala-Asp(OMe)-CH2F

References

1 Menendez JA, Lupu R. Fatty acid synthase and the lipogenic phenotype in cancer pathogenesis. *Nat Rev Cancer* 2007; **7**: 763–77.
2 Kuhajda FP. Fatty acid synthase and cancer: new application of an old pathway. *Cancer Res* 2006; **66**: 5977–80.
3 Brusselmans K, De Schrijver E, Verhoeven G, Swinnen JV. RNA interference-mediated silencing of the acetyl-CoA-carboxylase-alpha gene induces growth inhibition and apoptosis of prostate cancer cells. *Cancer Res* 2005; **65**: 6719–25.
4 Mashima T, Seimiya H, Tsuruo T. De novo fatty acid synthesis and related pathways as molecular targets for cancer therapy. *Br J Cancer* 2009; **100**: 1369–72.
5 Coleman RA, Lewin TM, Van Horn CG, Gonzalez-Baro MR. Do long-chain acyl-CoA synthetases regulate fatty acid entry into synthetic versus degradative pathways? *J Nutr* 2002; **132**: 2123–6.
6 Cao Y, Pearman AT, Zimmerman GA, McIntyre TM, Prescott SM. Intracellular unesterified arachidonic acid signals apoptosis. *Proc Natl Acad Sci U S A* 2000; **97**: 11280–5.
7 Yamashita Y, Kumabe T, Cho YY *et al.* Fatty acid induced glioma cell growth is mediated by the acyl-CoA synthetase 5 gene located on chromosome 10q25.1-q25.2, a region frequently deleted in malignant gliomas. *Oncogene* 2000; **19**: 5919–25.
8 Cao Y, Dave KB, Doan TP, Prescott SM. Fatty acid CoA ligase 4 is up-regulated in colon adenocarcinoma. *Cancer Res* 2001; **61**: 8429–34.
9 Gassler N, Herr I, Schneider A *et al.* Impaired expression of acyl-CoA synthetase 5 in sporadic colorectal adenocarcinomas. *J Pathol* 2005; **207**: 295–300.
10 Mashima T, Oh-hara T, Sato S *et al.* p53-defective tumors with a functional apoptosome-mediated pathway: a new therapeutic target. *J Natl Cancer Inst* 2005; **97**: 765–77.
11 Fesik SW. Promoting apoptosis as a strategy for cancer drug discovery. *Nat Rev Cancer* 2005; **5**: 876–85.
12 Riedl SJ, Salvesen GS. The apoptosome: signalling platform of cell death. *Nat Rev Mol Cell Biol* 2007; **8**: 405–13.
13 Mashima T, Tsuruo T. Defects of the apoptotic pathway as therapeutic target against cancer. *Drug Resist Updat* 2005; **8**: 339–43.
14 Reed JC, Pellecchia M. Apoptosis-based therapies for hematologic malignancies. *Blood* 2005; **106**: 408–18.
15 Meng XW, Lee SH, Kaufmann SH. Apoptosis in the treatment of cancer: a promise kept? *Curr Opin Cell Biol* 2006; **18**: 668–76.
16 Letai AG. Diagnosing and exploiting cancer's addiction to blocks in apoptosis. *Nat Rev Cancer* 2008; **8**: 121–32.
17 Yang L, Mashima T, Sato S *et al.* Predominant suppression of apoptosome by inhibitor of apoptosis protein in non-small cell lung cancer H460 cells: therapeutic effect of a novel polyarginine-conjugated Smac peptide. *Cancer Res* 2003; **63**: 831–7.
18 Mashima T, Udagawa S, Tsuruo T. Involvement of transcriptional repressor ATF3 in acceleration of caspase protease activation during DNA damaging agent-induced apoptosis. *J Cell Physiol* 2001; **188**: 352–8.
19 Mashima T, Naito M, Tsuruo T. Caspase-mediated cleavage of cytoskeletal actin plays a positive role in the process of morphological apoptosis. *Oncogene* 1999; **18**: 2423–30.
20 Mashima T, Sato S, Sugimoto Y *et al.* Promotion of glioma cell survival by acyl-CoA synthetase 5 under extracellular acidosis conditions. *Oncogene* 2009; **28**: 9–19.
21 Heitjan DF, Manni A, Santen RJ. Statistical analysis of in vivo tumor growth experiments. *Cancer Res* 1993; **53**: 6042–50.
22 R development core team. R: a language and environment for statistical computing. R foundation for statistical computing. Vienna: 2007 (URL: http://www.R-project.org).
23 Kim JH, Lewin TM, Coleman RA. Expression and characterization of recombinant rat Acyl-CoA synthetases 1, 4, and 5. Selective inhibition by triacsin C and thiazolidinediones. *J Biol Chem* 2001; **276**: 24667–73.
24 Lewin TM, Kim JH, Granger DA, Vance JE, Coleman RA. Acyl-CoA synthetase isoforms 1, 4, and 5 are present in different subcellular membranes in rat liver and can be inhibited independently. *J Biol Chem* 2001; **276**: 24674–9.
25 Jurgensmeier JM, Xie Z, Deveraux Q, Ellerby L, Bredesen D, Reed JC. Bax directly induces release of cytochrome c from isolated mitochondria. *Proc Natl Acad Sci U S A* 1998; **95**: 4997–5002.
26 Martin AG, Fearnhead HO. Apocytochrome c blocks caspase-9 activation and Bax-induced apoptosis. *J Biol Chem* 2002; **277**: 50834–41.
27 Yoshida A, Pourquier P, Pommier Y. Purification and characterization of a Mg^{2+}-dependent endonuclease (AN34) from etoposide-treated human leukemia HL-60 cells undergoing apoptosis. *Cancer Res* 1998; **58**: 2576–82.
28 Perkins CL, Fang G, Kim CN, Bhalla KN. The role of Apaf-1, caspase-9, and bid proteins in etoposide- or paclitaxel-induced mitochondrial events during apoptosis. *Cancer Res* 2000; **60**: 1645–53.
29 Lowe SW, Cepero E, Evan G. Intrinsic tumour suppression. *Nature* 2004; **432**: 307–15.
30 Tsuruo T, Naito M, Tomida A *et al.* Molecular targeting therapy of cancer: drug resistance, apoptosis and survival signal. *Cancer Sci* 2003; **94**: 15–21.
31 Fulda S, Debatin KM. Extrinsic versus intrinsic apoptosis pathways in anticancer chemotherapy. *Oncogene* 2006; **25**: 4798–811.
32 Mashek DG, McKenzie MA, Van Horn CG, Coleman RA. Rat long chain acyl-CoA synthetase 5 increases fatty acid uptake and partitioning to cellular triacylglycerol in McArdle-RH7777 cells. *J Biol Chem* 2006; **281**: 945–50.
33 Ott M, Zhivotovsky B, Orrenius S. Role of cardiolipin in cytochrome c release from mitochondria. *Cell Death Differ* 2007; **14**: 1243–7.
34 Sung YK, Hwang SY, Park MK *et al.* Fatty acid-CoA ligase 4 is overexpressed in human hepatocellular carcinoma. *Cancer Sci* 2003; **94**: 421–4.

Supporting Information

Additional Supporting Information may be found in the online version of this article:

Fig. S1. Acyl-CoA synthetase (ACS) enzyme activity of the delta L mutant. ACS activity in mock-, ACSL5-, and delta L–transduced SF268 cells was measured as described in 'Materials and Methods'.

Fig. S2. Localization of the ACSL5 delta L mutant in SF268 cells. The delta L mutant of ACSL5 (FLAG) and a mitochondria marker, cytochrome c (Cyto c), were detected by indirect immunofluorescence staining of delta L–transduced SF268 cells with anti-FLAG M2 (red) and anticytochrome c (green) antibodies, respectively. DAPI staining of DNA is shown in blue.

Fig. S3. Effect of acyl-CoA synthetase (ACS) inhibition on mitochondria-dependent apoptosis pathway regulators. Mock- and ACSL5-transduced SF268 cells were left untreated or were treated with 1-μM Triacsin c in the absence or presence of a 50 μM caspase inhibitor, Z-Val-Ala-Asp(OMe)-CH2F (Z-VAD), for 36 h. Expression of proteins that regulate cytochrome c release from mitochondria (Bcl-2, Bcl-XL, and Bax) was analyzed by western blot.

doi: 10.1111/j.1349-7006.2009.01203.x

ANTICANCER RESEARCH *29*: 1059-1066 (2009)

Pharmacological Interplay between Breast Cancer Resistance Protein and Gefitinib in Epidermal Growth Factor Receptor Signaling

KAZUHIRO KATAYAMA[1*], KAZUHIKO SHIBATA[1*], JUNKO MITSUHASHI[1,2], KOHJI NOGUCHI[1] and YOSHIKAZU SUGIMOTO[1,2]

[1]*Division of Chemotherapy, Graduate School of Pharmaceutical Sciences, Keio University, Tokyo;*
[2]*Division of Gene Therapy, Cancer Chemotherapy Center, Japanese Foundation for Cancer Research, Tokyo, Japan*

Abstract. *Background: It has been previously shown that gefitinib reverses breast cancer resistance protein (BCRP)-mediated drug resistance. Here, the impact of BCRP on gefitinib-mediated inhibition in epidermal growth factor receptor (EGFR) signaling is evaluated. Materials and Methods: Sensitivity to gefitinib was determined by growth inhibition assay, and intracellular gefitinib levels were measured with HPLC. Western blotting was performed to detect EGFR signaling molecules. Results: BCRP reduced intracellular gefitinib levels and attenuated inhibitory activities of gefitinib to EGF-dependent EGFR signalings including downstream MAPK and Akt pathways in gefitinib-sensitive PC-9 cells. However, gefitinib did not inhibit MAPK and Akt signalings in KB-3-1 and HCT-116 cells, and BCRP-mediated gefitinib-resistance shown in PC-9 cells was not observed in gefitinib-insensitive KB-3-1 and HCT-116 cells. Conclusion: BCRP transports gefitinib and suppresses its inhibitory effects on EGFR phosphorylation. However, effects of BCRP on gefitinib activity in the EGFR signaling and on gefitinib-resistance were limited in the gefitinib-sensitive cells only.*

*Both authors contributed equally to this work.

Abbreviations: ABC, ATP-binding cassette; BCRP, breast cancer resistance protein; ATP, adenosine triphosphate; EGFR, epidermal growth factor receptor; ERK, extracellular signal-regulated kinase; HPLC, high performance liquid chromatography; NSCLC, non-small cell lung cancer.

Correspondence to: Yoshikazu Sugimoto, Division of Chemotherapy, Graduate School of Pharmaceutical Sciences, Keio University, 1-5-30 Shibakoen, Minato-ku, Tokyo 105-8512, Japan. Tel: +81 3 5400 2670, Fax: +81 3 5400 2669, e-mail: sugimoto-ys@pha.keio.ac.jp

Key Words: BCRP/ABCG2, gefitinib, HPLC, EGFR.

ATP-binding cassette (ABC) transporters, including breast cancer resistance protein (BCRP)/ABCG2, P-glycoprotein (P-gp)/ABCB1 and multidrug resistance-related protein 1 (MRP1)/ABCC1, are involved in multidrug resistance phenotypes (1). These proteins function by pumping out various structurally unrelated agents using ATP hydrolysis energy. BCRP is a half-molecule ABC transporter with an NH_2-terminal ATP-binding site and a COOH-terminal transmembrane domain (2-6). BCRP forms homodimers *via* disulfide bridges between Cys603, a residue on the third outer-membrane domain of the BCRP monomer (7, 8). Homodimeric BCRP acts as an efflux pump for various anticancer agents, including 7-ethyl-10-hydroxycamptothecin (SN-38), 9-aminocamptothecin and mitoxantorone. BCRP prevents intracellular accumulation of such compounds and thereby decreases their cytotoxic effects (5, 9-11). BCRP is expressed in various normal human tissues and cells, including the placenta, liver, kidney and small intestine, and exports natural compounds, including sulfated estrogens and flavonoids (12-15).

Gefitinib is an epidermal growth factor receptor (EGFR) inhibitor that functions by competitively binding to the ATP-binding domain, and is clinically used for treating non-small cell lung cancer (NSCLC) patients (16, 17). In particular, this drug is more effective against tumor growth in NSCLC harboring deletions in exon 19 (del E746-T753) and/or point mutations in exon 21 (L858R and L861Q) of EGFR (16, 17). Gefitinib markedly inhibits epidermal growth factor (EGF)-mediated autophosphorylation of EGFR in various EGFR-expressing human cancer cell lines and xenografts, and effectively suppresses important signal transduction pathways that are implicated in the proliferation and survival of tumor cells (16, 17).

In a previous study, it has been shown that gefitinib reverses the BCRP-mediated anticancer drug resistance phenotype (18). In addition, it was shown that *BCRP*-transduced human lung cancer PC-9 (PC-9/BCRP) cells show gefitinib resistance, whereas *BCRP*-transduced human myelogenous leukemia K562

0250-7005/2009 $2.00+.40

(K562/BCRP) cells do not (19). To better understand the mechanisms underlying gefitinib resistance by BCRP, the effects of BCRP upon gefitinib uptake and efflux and the consequences of this for the inhibition of EGFR downstream signaling were examined. It is demonstrated that BCRP-expressing cells show lower accumulation and higher efflux of gefitinib than their parental cells regardless of the cell types tested. However, the data show that BCRP-expressing cells show gefitinib resistance only when the cells are sensitive to gefitinib.

Materials and Methods

Reagents. Gefitinib was kindly provided by AstraZeneca UK Ltd. (London, UK). EGF was obtained from Sigma (St. Louis, MO, USA). Rabbit anti-BCRP polyclonal antibody 3488 was prepared in the laboratory as described previously (7). Other primary antibodies were purchased as follows: mouse anti-MDR1+3 monoclonal antibody (C219) was sourced from Zymed (South San Francisco, CA, USA), mouse anti-GAPDH monoclonal antibody was obtained from Chemicon (Temecula, CA, USA), mouse anti-EGFR monoclonal antibody was purchased from Santa Cruz Biotechnology (Santa Cruz, CA, USA), and rabbit anti-p44/p42, anti-phospho-p44/p42 (Thr202/Tyr204), anti-Akt and anti-phospho-Akt (Ser473) polyclonal antibodies, and mouse anti-phospho-EGFR (Tyr1068) monoclonal antibody were supplied by Cell Signaling Technology (Danvers, MA, USA).

Cells and drug sensitivity assay. Human NSCLC PC-9, human epidermoid carcinoma KB-3-1 and human colorectal tumor HCT-116 cells were cultured in DMEM supplemented with 7% fetal bovine serum at 37°C in 5% CO_2. PC-9/BCRP, KB/BCRP and HCT-116/BCRP cells were established by the transduction of PC-9, KB-3-1 and HCT-116 cells, respectively, with a HaBCRP retrovirus harboring a Myc-tagged human *BCRP* cDNA in the Ha retrovirus vector as described previously (7). The effects of anticancer agents on the cells were evaluated by measuring cell growth inhibition after incubation at 37°C for 5 days in presence of various concentrations of the drugs. Cell numbers were determined with a Coulter counter. The IC_{50} values (the dosage of drugs at which a 50% inhibition of cell growth was achieved) were determined from the growth inhibition curve.

Western blot analysis. Western blot analysis was performed as reported previously (7, 20). Briefly, cell lysates were solubilized with sample buffer (2% SDS, 50 mmol/L Tris-HCl (pH 8.0), 0.2% bromophenol blue, 5% 2-mercaptoethanol) with boiling for 10 min at 70°C (to evaluate ABC transporters) or for 5 min at 100°C (to assess EGFR signaling). The lysates were then separated by SDS-PAGE using 5-20% gradient gel, and transferred onto nitrocellulose membranes. The membranes were incubated with primary antibodies followed by horseradish peroxidase-conjugated sheep anti-mouse or anti-rabbit secondary antibodies (Amersham Biosciences Corp., Piscataway, NJ, USA). Bands were visualized using the ECL (enhanced chemiluminescence) Plus detection kit (Amersham Biosciences Corp.).

Fluorescence-Activated Cell Sorting (FACS). The expression levels of BCRP on cell surfaces were determined by FACS analysis as described before (20). In brief, cells were incubated with or without a biotinylated human-specific monoclonal antibody raised against BCRP (eBioscience, San Diego, CA, USA) (100 μg/mL). These cells were then washed and incubated with R-phycoerythrin-conjugated streptavidin (400 μg/mL; Becton Dickinson and Company, Franklin Lakes, NJ, USA). Fluorescence staining levels were detected using FACSCalibur instrument (Becton Dickinson and Company).

High performance liquid chromatography (HPLC) analysis. Trypsinized cells (3×10^6) were incubated with 0.5 μmol/L gefitinib for 2, 5 or 10 min at 37°C for uptake experiments and then washed twice with ice-cold PBS. For efflux experiments, the cells were incubated with 0.5 μmol/L gefitinib for 10 min, washed twice with ice-cold PBS, further incubated in gefitinib-free flesh normal growth medium for 2, 5 or 10 min at 37°C and immediately washed twice with ice-cold PBS. Cells were lysed with ethanol, vortexed and centrifuged at 14,000 rpm for 20 min at 4°C. The cell extracts were chromatographed on a 4.6 mm x 250 mm ID Inertsil ODS3 column (GL Sciences Inc., Tokyo, Japan) with 80% acetonitrile: 20% aqueous ammonium acetate at a flow rate of 1 mL/min. A Shimadzu SPD-20A mass spectrometer was used for subsequent detection of gefitinib at a measuring wavelength of 332 nm.

Results

Characterization of BCRP-transduced PC-9, KB-3-1 and HCT-116 cells. It has been previously reported that gefitinib reverses BCRP-mediated anticancer drug resistance (18). To examine whether BCRP directly transports gefitinib in the current study, three different cell lines and BCRP-transduced cells derived from them were used. The expression levels of EGFR protein in these cell lines were confirmed by Western blotting. PC-9, PC-9/BCRP, KB-3-1 and KB/BCRP cells expressed significant amounts of EGFR, however, HCT-116 and HCT-116/BCRP cells expressed only marginal levels of EGFR (Figure 1A). BCRP transduction did not affect EGFR expression in any cell types. The expression of BCRP was then confirmed by both Western blotting and FACS (Figure 1B and C). Further, P-gp expression was also confirmed by Western blotting in each cell line (Figure 1B). BCRP was not detectable in the parental PC-9, KB-3-1 and HCT-116 cells, whereas PC-9/BCRP, KB/BCRP and HCT-116/BCRP cells expressed significant amounts of exogenous BCRP. The BCRP expression levels of PC-9/BCRP and HCT-116/BCRP cells were higher than those of the KB/BCRP cells, but none of these cell types expressed P-gp. Furthermore, FACS analysis revealed that BCRP was expressed on the cell surface in the transduced cells only.

PC-9/BCRP but not KB/BCRP or HCT-116/BCRP cells are resistant to gefitinib. Drug sensitivity assays were performed for topotecan in PC-9/BCRP, KB/BCRP and HCT-116/BCRP cells (Table I). All of the *BCRP*-transduced cells showed much higher resistance to topotecan compared with the parental cells, indicating that BCRP is active in these three transduced cell lines. Their sensitivity to gefitinib was then examined. The IC_{50} values of PC-9 and PC-9/BCRP cells to gefitinib were determined to be 4 and 27 nmol/L, respectively, and therefore PC-9/BCRP cells showed an approximately 7-fold higher resistance to gefitinib than the parental PC-9 cells. In contrast,

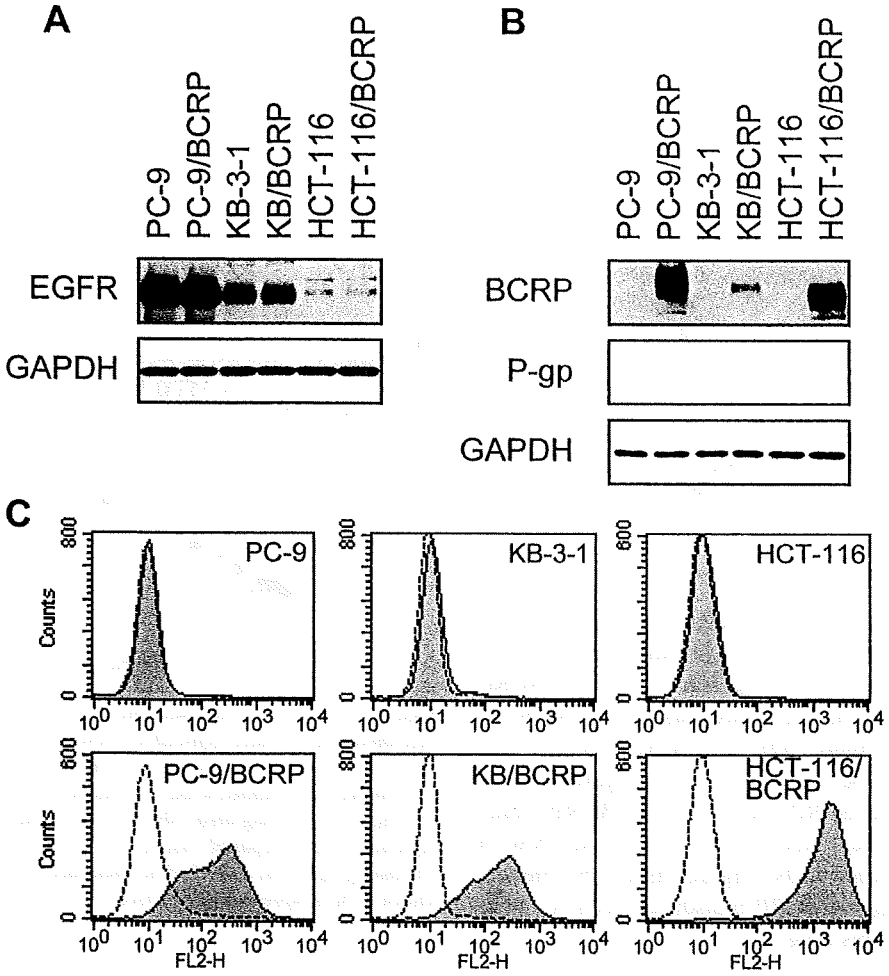

Figure 1. *Analysis of the expression levels of EGFR, BCRP and P-gp in BCRP-transduced cells. (A, B) Cell lysates (10 μg/lane) were resolved by SDS-PAGE and expression levels of EGFR or GAPDH were detected by Western blotting using anti-EGFR polyclonal antibody or anti-GAPDH monoclonal antibody, respectively (A). The expression levels of BCRP, P-gp or GAPDH were detected by anti-BCRP (3488), anti-P-gp (C219) or anti-GAPDH antibodies, respectively (B). (C) Cells were harvested with trypsin, washed with PBS and incubated with (closed areas) or without (open areas) a biotinylated anti-BCRP antibody. The cells were incubated with R-phycoerythrin–conjugated streptavidin. BCRP expression levels were determined using FACSCalibur instrument.*

KB/BCRP and HCT-116/BCRP cells did not show any resistance to gefitinib compared with their respective parental cells. The IC_{50} values for KB-3-1 and HCT-116 cells were approximately 2 and 3 μmol/L respectively, and were much higher than those for PC-9 cells. These data indicate that BCRP confers gefitinib-resistance in gefitinib-sensitive PC-9 cells while it did not in gefitinib-insensitive KB-3-1 or HCT-116 cells.

Lower accumulation of Gefitinib in BCRP-transduced cells. Both the uptake and efflux of gefitinib were examined in *BCRP*-transduced cells and their parental cells. HPLC was used to determine intracellular gefitinib levels with a calibration curve (Figure 2). In the uptake experiments, cells were incubated with 0.5 μmol/L gefitinib for 2, 5 or 10 min. Intracellular gefitinib was then extracted from the cells and quantified by HPLC (Figure 3A-C). The intracellular gefitinib levels almost reached a plateau phase at 2 min after treatment with this drug in each cell line. Significantly, the intracellular gefitinib levels in each *BCRP*-transduced cell line were much lower than those in the corresponding parental cells. Actually, at 10 min incubation period, the intracellular gefitinib levels in the PC-9/BCRP and KB/BCRP cells were approximately 2-fold lower than those in the PC-9 and KB-3-1 cells, respectively (Figure 3A and B). The intracellular levels of gefitinib in the HCT-116/BCRP cells were approximately two-thirds of those in the HCT-116 cells (Figure 3C). In the efflux experiments, the cells were incubated with 0.5 μmol/L gefitinib for 10 min, washed and

Table I. *Drug resistance characteristics of BCRP-transduced cells*.*

Cell line	Topotecan		Gefitinib	
	IC_{50} (nmol/L)	RR#	IC_{50} (nmol/L)	RR#
PC-9	11.4±0.42		3.67±0.56	
PC-9/BCRP	206±17.4	18.0	26.8±4.4	7.3
KB-3-1	21.4±0.01		2310±72	
KB-/BCRP	84.1±0.55	3.9	2200±140	0.95
HCT-116	3.67±0.15		3140±410	
HCT-116/BCRP	49.9±0.98	13.6	3030±410	0.96

*Parental or *BCRP*-transduced cells were cultured for 5 days with increasing concentrations of topotecan or gefitinib. Cell numbers were counted with a Coulter counter, and IC_{50} values were determined. #Relative resistance. These values were obtained by dividing the IC_{50} values of the BCRP-transduced cells by the IC_{50} values of the corresponding parental cells.

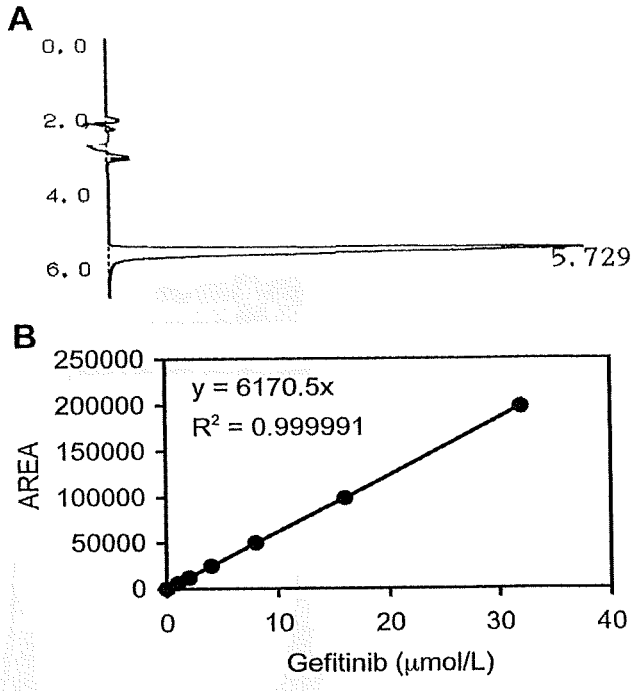

Figure 2. *Detection and quantification of gefitinib by HPLC. (A) Retention time of eluted gefitinib is shown in Y-axis, and eluted gefitinib peak is shown in X-axis in the chromatographic pattern. (B) A calibration curve plotted using the indicated concentrations of gefitinib and the corresponding areas obtained by chromatography. Each dose of gefitinib was prepared using a two-fold dilution series and chromatographed as described in Materials and Methods. The data was shown to be a representative subset.*

then incubated in gefitinib-free normal growth medium for 2, 5 or 10 min. After 2 min incubation in gefitinib-free medium, 49% of the gefitinib that had incorporated into PC-9/BCRP cells was released, whereas this figure was only 11% in the parental PC-9 cells (Figure 3D). Similarly, during 2 min incubation 72% and 61% of the accumulated gefitinib was released from the KB/BCRP and HCT-116/BCRP cells, respectively, whereas these amounts were 46% and 38% in the corresponding parental cells (Figure 3E and F). Hence, lower uptake of gefitinib in *BCRP*-transduced cells is due to an increased efflux of this drug.

Effects of BCRP expression on the inhibition of EGFR downstream signaling by gefitinib. Next, examination on whether the inhibitory effects of gefitinib upon EGFR signaling were affected by BCRP expression was performed. To test this, PC-9 and PC-9/BCRP cells were treated with various concentrations of gefitinib followed by EGF treatment in absence of serum (Figure 4A). The levels of phosphorylated EGFR were reduced over 0.1 nmol/L gefitinib in PC-9 cells but were unaffected until 30 nmol/L in PC-9/BCRP cells. Consistently, gefitinib downregulated EGF-dependent phosphorylation of extracellular signal-regulated kinase (ERK) at a dose of 0.1 nmol/L in PC-9 cells but only did so in PC-9/BCRP cells at dose of over 300 nmol/L. The downregulation of Akt phosphorylation by gefitinib in PC-9 and PC-9/BCRP cells was observed at concentrations of 0.1 and 100 nmol/L, respectively. BCRP thus confers resistance to the inhibitory effects of gefitinib on EGFR signaling in PC-9/BCRP cells.

The EGFR signaling status of KB-3-1, KB/BCRP, HCT-116 and HCT-116/BCRP cells after gefitinib exposure in a concentration range of 0.1-30,000 nmol/L (Figures 4B and C) was also examined. Regarding phosphorylated EGFR levels, KB/BCRP and HCT-116/BCRP cells were found to be resistant to gefitinib compared with the corresponding parental cells. However, exogenous BCRP expression did not confer resistance to the effects of gefitinib upon the EGFR downstream signaling pathways, including ERK and Akt activities in KB/BCRP and HCT-116/BCRP cells. The phosphorylated ERK and Akt levels were unaffected by a much higher concentration of gefitinib (~30 μmol/L) in both *BCRP*-transduced and parental cells. Taken together, the presented data therefore indicate that BCRP exports gefitinib from all cell types but BCRP-mediated gefitinib-resistance is acquired in gefitinib-responsive cells only.

Discussion

It has been previously demonstrated that gefitinib reverses BCRP-mediated anticancer drug resistance in K562 and murine lymphocytic leukemia P388 cells, suggesting gefitinib as a competitor for other BCRP substrates including SN-38 and mitoxantrone (18). In addition, it has been shown that PC-9/BCRP cells show gefitinib resistance but K562/BCRP cells do not (18, 19). K562 cells are not a suitable for these studies because they do not express EGFR.

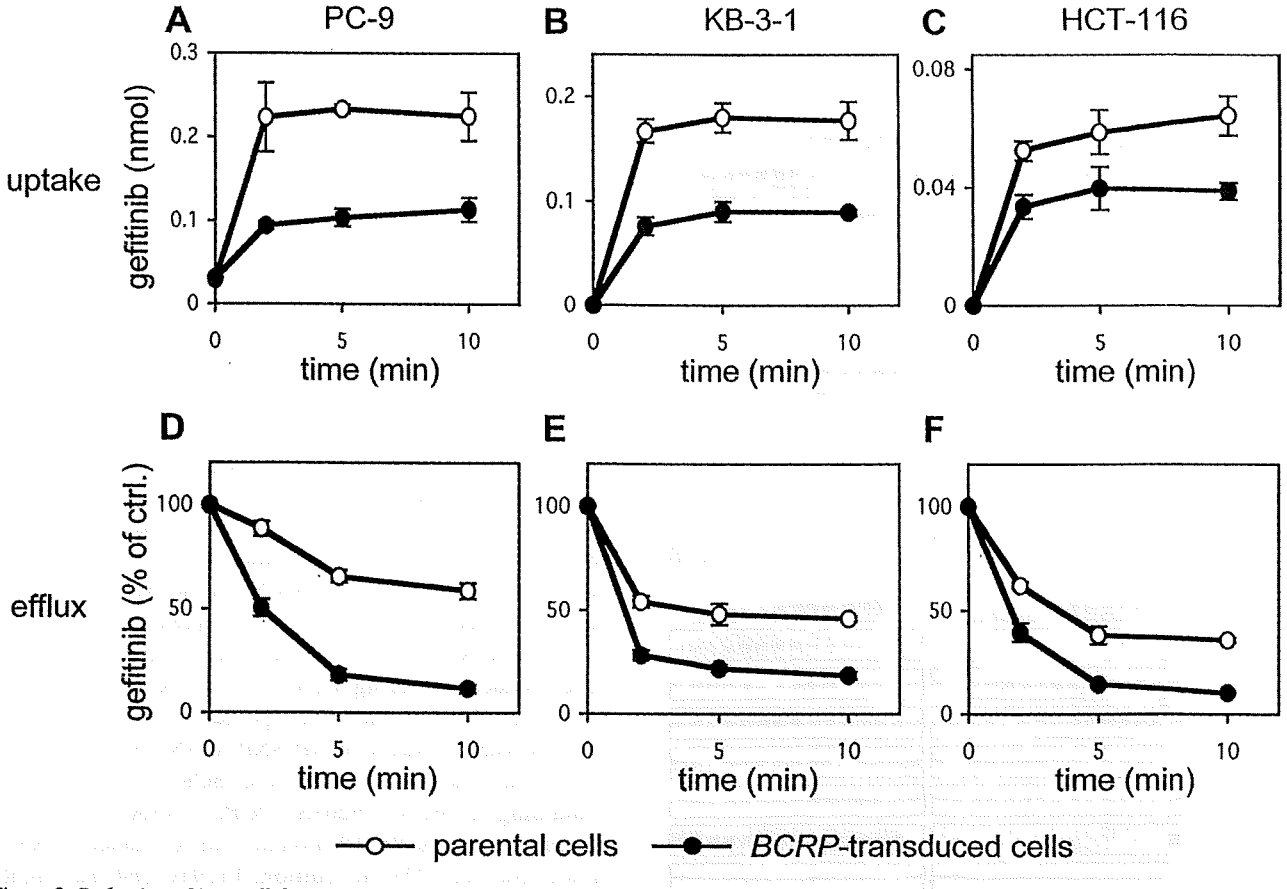

Figure 3. *Reduction of intracellular gefitinib concentration in BCRP-transduced cells. (A-C) Uptake of gefitinib. The BCRP-transduced cells (closed circles) or their respective parental cells (open circles) were treated with 0.5 μmol/L gefitinib for 2, 5 or 10 min at 37°C. At each time point, cells were lysed with ethanol, and cell extracts were chromatographed by HPLC to detect intracellular gefitinib. Intracellular gefitinib concentration is shown as the levels per 3×10^6 cells and was calculated from a pre-determined calibration curve. Data points are measurements of the mean±SD from triplicate determinations. (D-F) Efflux of gefitinib. The BCRP-transduced cells (closed circles) or their respective parental cells (open circles) were treated with 0.5 μmol/L gefitinib for 10 min at 37°C. Cells were further incubated in gefitinib-free normal growth medium for 2, 5 or 10 min. Cells were lysed with ethanol, and cell extracts were chromatographed as described above. The data shown are the relative amounts of gefitinib compared with the control (treatment with gefitinib only at the 0 time point) and are the mean±SD from triplicate determinations.*

In the present study, three cancer cell lines that express EGFR (Figure 1A) and their respective *BCRP*-transduced cells were used to further examine the mechanisms of BCRP-dependent gefitinib resistance. PC-9 cells were highly sensitive to gefitinib with an IC_{50} of approximately 4 nmol/L (Table I). It has been demonstrated that gefitinib appreciably inhibits EGFR mutants harboring deletions in exon 19 or point mutations in exon 21, when compared with the wild-type protein (16, 17). *In vitro* studies have indicated that gefitinib may exert much higher inhibitory effects against mutant EGFR variants (16, 17, 21). Consistently, PC-9 cells harbor a deletion in EGFR (del E746-A750) (22), and PC-9 cells are highly gefitinib-sensitive. BCRP was found to suppress the intracellular accumulation of gefitinib by promoting its efflux in all three cell lines tested in the present study (Figure 3). The low levels of accumulation of gefitinib in PC-9/BCRP cells will reduce cytotoxic effects against EGFR downstream signaling compared with PC-9 cells. Since EGFR downstream signalings, MAPK and Akt pathways, were also highly sensitive to gefitinib in PC-9 cells (Figure 4A), BCRP would be able to confer resistance to gefitinib in this gefitinib-sensitive cells.

On the other hand, KB-3-1 and HCT-116 cells were less sensitive to gefitinib with IC_{50} values of approximately 2 and 3 μmol/L, respectively (Table I), and their gefitinib-insensitivities were no longer affected by BCRP. Unlike PC-9 cells, cells that are marginally responsive to gefitinib, including KB-3-1 and HCT-116 cells which harbor wild-type EGFR, are not dependent on EGFR signaling for cell growth (23). Actually, cell growth and survival signaling such as

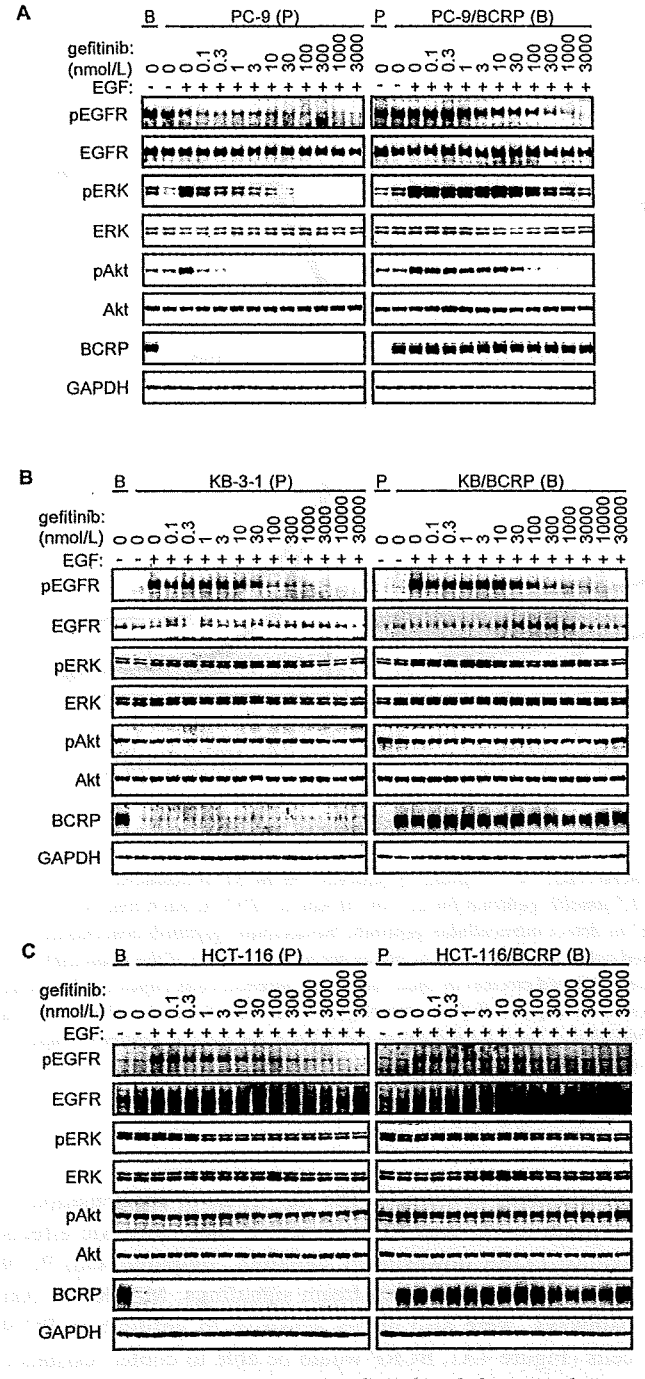

Figure 4. *Suppression of the gefitinib-mediated down-regulation of EGFR signaling in the BCRP-transduced cells. PC-9 and PC-9/BCRP cells (A), KB-3-1 and KB/BCRP cells (B), or HCT-116 and HCT-116/BCRP cells (C) were cultured in medium without serum for one hour and then treated with the indicated concentrations of gefitinib for 3 h under conditions of serum starvation. The cells were then treated with 100 μg/L of EGF for 15 min and harvested immediately. Cell extracts were used in Western blotting with anti-phospho-EGFR (Tyr1068), anti-EGFR, anti-phospho-ERK (Thr202/Tyr204), anti-ERK, anti-phospho-Akt (Ser473), anti-Akt, anti-BCRP or anti-GAPDH antibodies. P, parental cells; B, BCRP-transduced cells.*

MAPK and Akt pathways of KB-3-1 and HCT-116 cells were gefitinib-insensitive and looked to be independent of EGFR phosphorylation (Figures 4B and C). Therefore, it is presumed that BCRP-mediated gefitinib efflux and restoration of EGFR phosphorylation would not confer gefitinib-resistance in gefitinib-insensitive cells.

ERK1/2 and Akt are central molecules during EGF-mediated cell growth and survival. EGF activates ERK1/2 and Akt in a phosphorylation-dependent manner *via* EGFR activation (24). However, the status of MAPK and Akt pathways will be different in each cell type, which may be due to the presence of *EGFR* gene mutations and the dependency of a particular cell type upon EGFR signaling for their survival and growth. The activities of these factors are therefore important parameters when monitoring gefitinib therapy.

In addition, these studies reveal that BCRP expression would modulate gefitinib sensitivity in highly gefitinib-sensitive cancer cells. Concerning BCRP activity, single nucleotide polymorphisms (SNPs) in the *BCRP* gene have been reported to determine its expression levels and transport activities (25-27). The expression levels of *BCRP* gene products harboring a C421A (Q141K) SNP are 5-fold lower than those of the wild-type gene, and the resistance of cells with a C421A *BCRP* SNP to SN-38 is also 5-fold lower than those with wild-type BCRP (25, 27). Cells containing a T623C (F208S) *BCRP* cDNA express only marginal levels of BCRP protein, and resistance to SN-38 is not observed (27). In addition, T1291C (F431L) BCRP-transfectants express two BCRP products of 65 kDa and 70 kDa, and resistance to SN-38 in these cells is significantly lower than wild-type *BCRP*-transfectants (27). Hence, SNPs affect the BCRP protein expression levels and thereby *BCRP* SNP(s) may also affect gefitinib transport and resistance to it. Indeed, Cusatis *et al.* reported that C421A *BCRP* SNP was associated with a high incidence of diarrhea in gefitinib-treated patients (28). It will therefore be important to evaluate *BCRP* SNPs in any future gefitinib therapy designs.

Overall, it has been hereby clarified that BCRP transports gefitinib. In cells that depend on EGFR signaling for their growth, the expression of BCRP was able to confer resistance to gefitinib-mediated cytotoxicity and inhibitory effects on EGFR signaling. It is reasoned that BCRP expression will affect the pharmacokinetics and pharmacodynamics of anticancer agents, and that BCRP is an important determining factor in the development and design of gefitinib-responsive cancer therapies.

Acknowledgements

We thank Akiko Ohmiya, Yoshimitsu Shimadate, Mei Sasaki and Yuki Iwamoto for their assistance. This study was supported by a Grant-in Aid for Cancer Research from The Ministry of Education, Culture, Sports, Science and Technology and the Ministry of Health, Labor and Welfare, Japan.